3 THE DECREPITATION OF HIGH TITANIA SLAGS

3.1 BACKGROUND

High titania slag is produced during the smelting of ilmenite in a furnace with a suitable carbonaceous reductant. In this process a large fraction of the iron content of the ilmenite is reduced to metallic iron. The remainder of the material collects in a high titania slag. The iron and slag are tapped through separate tapholes, with the titania slag being the higher value product. The slag is typically tapped into moulds that would yield approximately 20 ton slag blocks. After the slag is cooled, which can last approximately seven to ten days, it is crushed and milled to produce separate fine and coarse products. These products are used in the downstream processing for the production of titanium dioxide pigment. The fine slag product (-106 μm) is used by the sulphate processing route, while the coarser product (-850+106 μm) is used by the chloride processing route (van Niekerk, 1995). The coarse slag product (chloride grade) has a higher value than the fine slag product (sulphate grade). In 1998 the price for typical chloride grade slag was $ 386 per ton, while the price for typical sulphate grade slag was $ 340 per ton (Gambogi, 1998).

During the slag cooling process, which takes place under atmospheric conditions, severe decrepitation of the slag may occur. Decrepitation of the slag is detrimental, because an excess of fine material with average particle diameter of less than 106 μm is produced. It is important to produce a minimum amount of the fine slag, (which is sulphate grade slag, the lower value product) in order to maximize the income that can be derived from titania slag. This part of the investigation was undertaken to study the decrepitation of high titania slag to gain an understanding of the factors affecting decrepitation. In this study decrepitation is defined as the disintegration or crumbling of a material into component parts or smaller fragments. This is graphically illustrated in Figure 28. This figure shows a slag block (approximately 1 ton in size) that has partially decrepitated during the cooling process. The figure shows how the right side of the block has crumbled, with the decrepitated material lying in a heap at the base of the block. Figure 29 shows a micrograph of a typical slag sample that has shown no decrepitation behaviour, while Figure 30 shows a micrograph of a decrepitated slag sample. In comparing these two samples it is obvious that significant changes to the decrepitated material had taken place as shown by the extensive cracking of the decrepitated sample. These changes, and the reasons for these changes, will be investigated in this section.

3.2 LITERATURE SURVEY

3.2.1 DECREPITATION OF SLAGS

Decrepitation of slag is a fairly well known phenomenon, especially for steelmaking slags. Decrepitation of slag occurs due to phase and chemical changes in the slag, and the resultant volume changes associated with these phase changes. Examples of the decrepitation of slags are the following:

Figure 28: Side view of a slag block (tap 68) that had decrepitated (tap ladle in background)

Figure 29: Micrograph of a typical slag sample that has shown no decrepitation

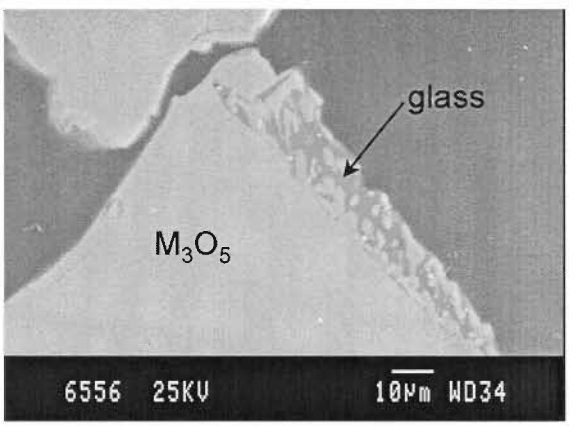

Figure 30: Micrograph of a slag sample that has undergone decrepitation (Sample DB157)

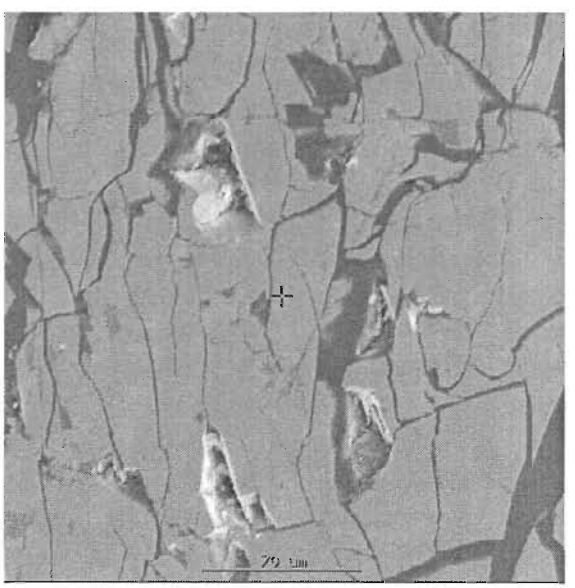

- The decrepitation of steelmaking slags due to an increase in volume of the free lime in the slag during hydration (Okamoto et. al., 1981; Noguchi et. al., 1980). This is particularly a problem in the aggregate industries. To overcome this problem the slag needs to undergo preliminary weathering in heaps prior to use. This allows some of the free lime to be converted to the hydroxide and carbonate (Juckes, 1991).
- A second well-known example is that of the disintegration on cooling of slag containing dicalcium silicate (Ca_2SiO_4). This disintegration is due to a structural transition from the β (monoclinic structure) to γ (rhombohedral structure) polymorph (Grzymek and Derdacka-Grzymek, 1990). From the data given by Grzymek and Derdacka-Grzymek (1990) it can be calculated that this transition is accompanied by an expansion in molar volume of approximately 10 per cent. According to the authors it seems that the addition of a cation with a small ionic radius can delay, or even inhibit the β to γ transition. Examples of these cations are B^{3+}, As^{3+} and Cr^{6+}. A patent has also been registered for the use of boron as a slag modifier to stabilise this type of slag (Harada and Tomari, 1991).

Very little (to the author's knowledge) has been published in the open literature on the oxidation and decrepitation behaviour of high titania slags. Vasyutinskiy and Movsesov (1965) studied the oxidation and grinding of a high titania slag containing 90.1 per cent TiO_2 and 3.47 per cent FeO. They concluded that in order to obtain the maximum reduction in strength of the slag, oxidation of the slag in the temperature region of 500 to 600 °C was required. Vasyutinskiy (1968) followed this up with a more in-depth study of the oxidation of a similar high titania slag. This slag consisted mainly of a M_3O_5 phase, with M denoting the cations present in the phase. This phase can best be represented as a $x[(Fe,Mg,Mn)O.2TiO_2].y[(Ti,Al,Cr)_2O_3.TiO_2]$ solid solution. The experimental results on the oxidation of the slag indicated the following three main stages.

- At temperatures of approximately 300 to 400 °C only slight structural changes in the M_3O_5 phase is observed. X-ray diffraction analysis indicated a distortion of the M_3O_5 crystal lattice.
- At temperatures of up to 750 °C the formation of anatase is observed.
- At higher temperatures the formation of rutile is observed.

The anatase to rutile transformation temperature can range between 400 and 1200 °C, depending on the source of the anatase and the nature of the impurities in it (Shannon and Pask, 1965). Decrepitation of these titania slags was explained by the oxidation of the M_3O_5 phase, resulting in the formation of anatase (Vasyutinskiy, 1968). As the density of anatase is less than the density of the M_3O_5 phase, this results in the rapid cracking of the slag.

Toromanoff and Habashi (1984) investigated the properties of high titania slags (produced at Sorel in Canada). Decrepitation of these slags during cooling was also observed. The slag consisted of a M_3O_5 phase, a glassy phase, rutile (TiO_2) and metallic iron globules. In this Sorel slag 13.1 mass per cent of the total Ti was present as Ti^{3+}. The decrepitation process was explained by the oxidation of the Ti^{3+} present in the slag by Fe^{2+} during the cooling process. It was postulated that this process occurs according to the following reaction:

$$Ti_2O_3 + FeO = 2TiO_2 + Fe^0 \ldots(K)$$
$$\Delta G^0_{1000\,°C} = -\,71.13\ kJ.mol^{-1}$$

Toromanoff and Habashi (1984) concluded that due to the difference in the coefficients of expansion of the metallic iron and the slag, the slag product cracks and decrepitates.

It is also known that ferrous and ferric pseudobrookite decompose at certain temperatures (Haggerty and Lindsley, 1970). It is possible that these decomposition reactions can contribute to the decrepitation of the high titania slags. The decomposition reactions are given below:

$$FeTi_2O_5 = FeTiO_3 + TiO_2 \quad [< 1150\ °C] \ldots(L)$$

$$Fe_2TiO_5 = Fe_2O_3 + TiO_2 \quad [< 585\ °C] \ldots(M)$$

Reid and Ward (1971) found that when a solid solution of Ti_3O_5 in $FeTi_2O_5$ was formed the tendency to decomposition decreased rapidly. It is also known that manganese and magnesium stabilize the M_3O_5 phase (Grey, Reid and Jones, 1974; Borowiec and Rosenqvist, 1981). This may counter the decomposition reactions or change the temperatures at which these occur.

Grey, Cranswick, et. al. (2000) studied the oxidation of synthetic anosovite ($Mg_{0.3}Ti_{2.7}O_5$) for various times at temperatures of 900 °C and lower. These workers found that after oxidation at temperatures below 300 °C, new phases were produced with the general composition of M_nO_{2n-1}, based on unit cell intergrowth of M_3O_5 and anatase structural elements. Structural homogeneity of these phases was restricted to regions of only 100 to 200 Å, due to the low driving force for ordering at these low temperatures. The composition of the dominant phase was found to be M_6O_{11}, although local regions corresponding to compositions of M_5O_9 and M_7O_{13} were also observed. With increasing temperature and oxidation time the x-ray diffraction patterns increasingly adopted the general features of the anatase pattern, although some differences were observed. After prolonged heating at 600 °C the x-ray diffraction patterns showed the start of the anatase to rutile transformation. At 900 °C the main products were rutile and M_3O_5, with traces of anatase. The powder X-ray diffraction patterns they obtained at the lower temperatures are shown in Figure 31, illustrating the differences obtained.

Teller et. al. (pp. 351-367, 1990) studied the thermal decomposition of two slag samples obtained by the high temperature reduction of ilmenite with carbon. The sample compositions were $Ti_{2.52}Fe_{0.33}Mn_{0.05}O_5$ and $Ti_{2.36}Fe_{0.33}Mg_{0.31}O_5$ respectively. Two distinct steps were observed in the decomposition of the metastable titanium-rich pseudobrookite phases. According to the authors the first step involves a phase transition that occurs above 500 °C. This transition is from a high temperature, ordered structure to a low temperature, dis-ordered pseudobrookite phase. This transition involves cation re-distribution whereby ferrous ions are transferred from the A site to the B site in the crystal structure. Before this reaction no iron was found in the B sites (See Table 5 for original distribution of cations in the two sites). At the same time titanium is transferred from the B site to the A site. In the second step the low temperature phase decomposes to metallic iron and an iron-containing, oxygen deficient titanium oxide with the rutile structure. In the light of the recent results obtained by Grey, Cranswick, et. al. (2000) with regard to the formation of a M_6O_{11} phase, and the results obtained in this study, this interpretation by Teller et. al. (pp. 351-367, 1990) needs revision.

3.2.2 PHASES AND PHASE RELATIONS APPLICABLE TO TITANIUM SLAGS AT LOW TEMPERATURES

As the decrepitation of high titania slags is expected to occur at temperatures below 1000 °C (based on practical observations and the available literature), it is relevant to study the phase assemblages that would be expected to be present at these temperatures. In this section the literature relevant to this is listed.

Figure 31: X-ray diffraction patterns for various products (from Grey, Cranswick, et. al., 2000)

(a) $Mg_{0.3}Ti_{2.7}O_5$
(b) Oxidation product from 30 minutes at 300 °C
(c) Oxidation product from 30 minutes at 400 °C
(d) Anatase

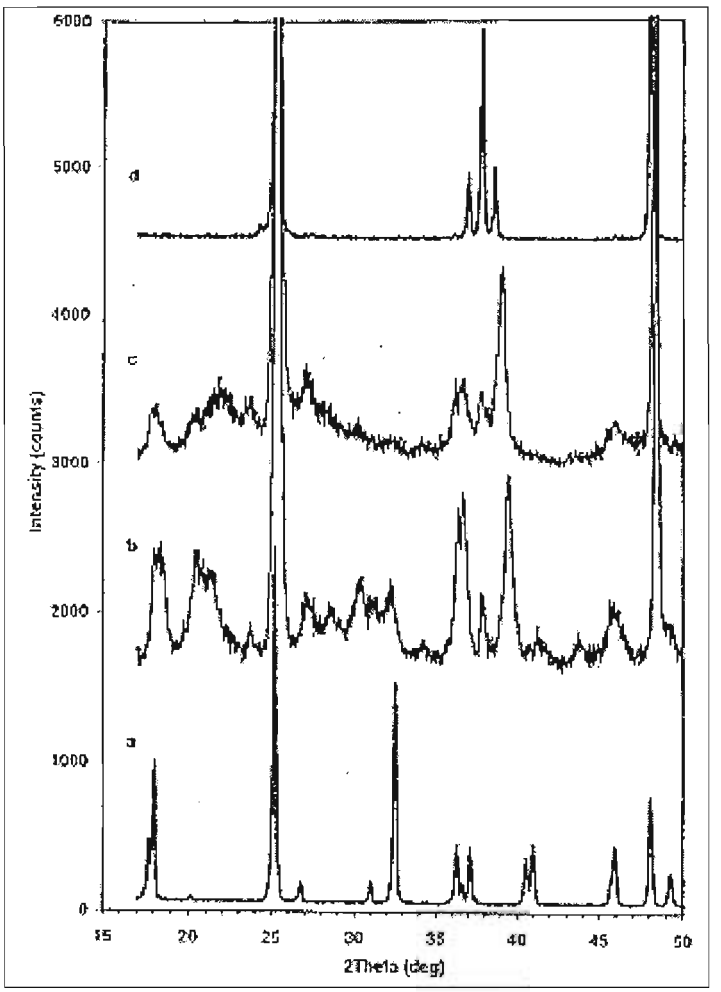

Various investigations have been carried out on oxidation reactions and phase relations in the Fe-Ti-O system at sub-solidus temperatures. These were done particularly to investigate the behaviour of ilmenite under oxidizing conditions. The following principal solid solution series are found in this system (Webster and Bright, 1961):

- The α-oxides ($Fe_mTi_{2-m}O_3$), also referred to as the M_2O_3 phases.
- The spinels ($Fe_nTi_{3-n}O_4$), also referred to as the M_3O_4 phases.
- The orthorhombic oxides ($Fe_pTi_{3-p}O_5$), also referred to as the M_3O_5 phases.
- The titanium oxide phases; rutile (TiO_2), anatase (TiO_2) and the Magnéli phases (Ti_xO_{2x-1})

Trace elements (for example magnesium, manganese, etc.) that are present in ilmenite smelting would also be included in the solid solution series, substituting for iron and titanium in the solid solutions. Information on the various iron and titanium phases present in the system is shown in Table 22.

Borowiec and Rosenqvist (1981) observed the phase relations and oxidation behaviour in the system Fe-Fe_2O_3-TiO_2 at temperatures below 1100 °C. A number of samples were made up by using pure chemical reagents in the required amounts. The samples were sealed in silica tubes under argon and reacted at various temperatures while the oxygen potentials were measured. On completion of the experiments the tubes were quenched and the phase combinations determined by X-ray diffraction analysis. Based on their results they compiled the isothermal phase diagrams shown in Figure 32 and Figure 33. The dashed lines show various values of the mole fraction of titanium ($N_{Ti} = n_{Ti}/(n_{Ti} + n_{Fe})$). This value remains constant for a specific sample whether it is oxidised or reduced. For titania slags the value for N_{Ti} is in the order of 0.90 (calculated for data shown in Table 12), showing that the TiO_2-rich corner of the Fe-Fe_2O_3-TiO_2 system is relevant to titania slags. The approximate position for $N_{Ti} = 0.9$ is also indicated in Figure 32.

For the oxidation of titania slag in the system Fe-Fe_2O_3-TiO_2 at 800 °C (Figure 32), the following phase assemblages could be expected with an increase in the extent of oxidation of a slag sample:

- Metallic iron, together with a succession of two Magnéli phases up to rutile, when all the titanium will be oxidised to Ti^{4+} (various three phase regions).
- Metallic iron, with rutile and ilmenite (three phase region).
- Rutile and α-oxide (two phase region).
- Rutile, α-oxide and pseudobrookite (three phase region).
- Rutile and pseudobrookite (two phase region). By increasing the extent of oxidation of the sample the amount of rutile relative to the amount of pseudobrookite increases. At the same time the amount of Fe^{3+} relative to Fe^{2+} also increases.
- The final phase assemblage will be rutile and Fe_2TiO_5, with all the iron oxidised to Fe^{3+}. For a slag with a value of 0.90 for N_{Ti}, the final phase composition will be 94.4 mole % (84.9 mass %) TiO_2 and 5.6 mole % (15.1 mass %) Fe_2TiO_5.

This reaction sequence does not allow for the presence of impurities, which may stabilise certain phases. From the phase diagram at 800 °C (Figure 32) it is not clear what oxygen partial pressure is required to obtain the final phase assemblage of Fe_2TiO_5 and rutile. For the three phase region (Rutile, α-oxide and pseudobrookite) the equilibrium oxygen potential in Figure 32 is shown as log P_{O2} = -11.41, which is much lower than that for air (log P_{O2} = -0.68). No data is however given for the two phase region, Fe_2TiO_5 and rutile. To obtain an indication of whether high titania slag oxidised in air would attain the Fe_2TiO_5 and rutile phase assemblage the oxygen potential for the following two reactions were calculated as a function of temperature:

$$2\ Ti_3O_5 + O_2 = 6\ TiO_2 \quad ...(N)$$

$$4\ FeTi_2O_5 + O_2 = 2\ Fe_2TiO_5 + 6\ TiO_2 \quad ...(O)$$

Table 22 : Mineralogical data on various iron and titanium phases that could potentially be present in the system under investigation

Stoichiometry	Chemical formula	Mineral name	Crystal system	Density ($g.cm^{-3}$)	Molecular mass ($g.mol^{-1}$)	Molar volume ($cm^3.mol^{-1}$)	References
M_2O_3	$FeTiO_3$	Ilmenite	Rhombohedral	4.72(m)	151.745	32.15	Hölzel (1989)
	Fe_2O_3	Hematite	Rhombohedral	5.26(m)	159.692	30.36	Hölzel (1989)
M_3O_4	Fe_2TiO_4	Ulvöspinel	Cubic	4.77(c)	223.592	46.87	Hölzel (1989)
	Fe_3O_4	Magnetite	Cubic	5.18(m)	231.539	44.70	Hölzel (1989)
M_3O_5	Fe_2TiO_5	Pseudobrookite (ferric)	Orthorhombic	4.39(m)	239.591	54.58	Hölzel (1989)
	$FeTi_2O_5$	Pseudobrookite (ferrous)	Orthorhombic	4.15(c)	231.644	55.82	Akimoto et. al. (1957), Grey and Ward (1973)
	$Fe_{0.5}Mg_{0.5}Ti_2O_5$	Armalcolite	Orthorhombic	3.92(c)	215.877	55.07	Hölzel (1989), Lind and Housley (1972)
	Ti_3O_5	Anosovite	Monoclinic	4.01(c)	223.697	55.78	Grey and Ward (1973)
M_5O_9	$Fe_2Ti_3O_9$	Pseudorutile	Hexagonal	4.01(c)	399.389	99.60	Hölzel (1989)
MO_2	TiO_2	Rutile	Tetragonal	4.23(m)	79.899	18.89	Hölzel (1989)
	TiO_2	Anatase	Tetragonal	3.90(m)	79.899	20.49	Hölzel (1989)

(c) – Calculated from crystallographic data
(m) – Measured data

Figure 32: Phase diagram for the system Fe-Fe_2O_3-TiO_2 at 800 °C. Compositions are in mol-units (From Borowiec and Rosenqvist, 1981)

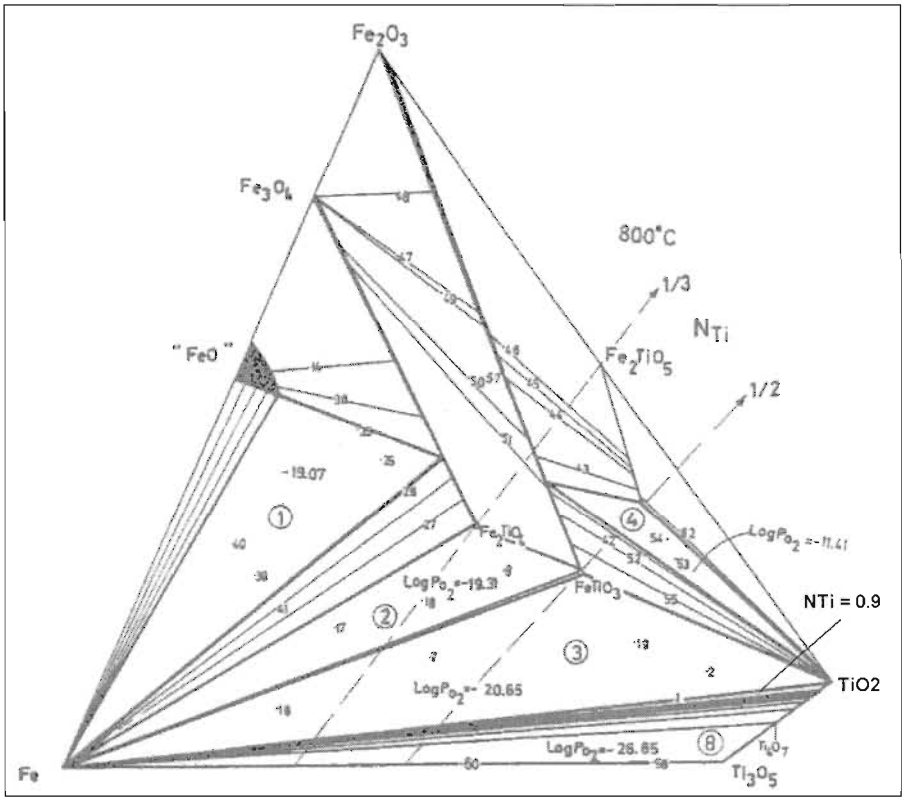

Figure 33 : Phase diagram for the system Fe-Fe_2O_3-TiO_2 at approximately 700 °C. Compositions are in mol-units (From Borowiec and Rosenqvist, 1981)

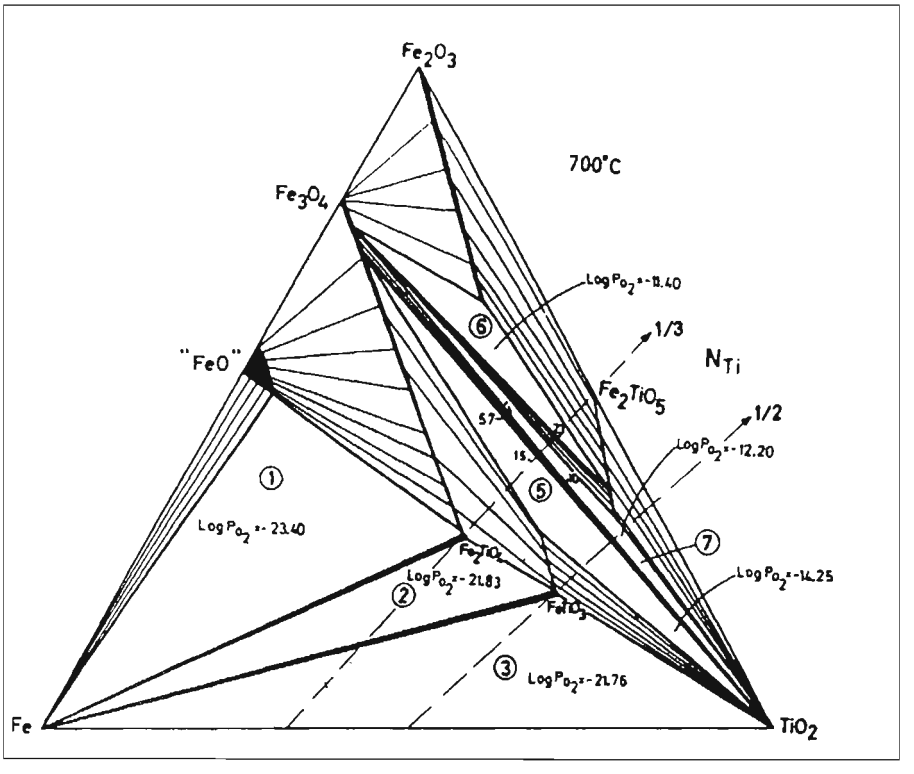

$FeTi_2O_5$ and Ti_3O_5 were used, as these two M_3O_5 phases essentially represent the two end members of the M_3O_5 solid solution obtained in high titania slags. Gibbs free energy data for each compound was obtained from the FACT thermodynamic database (2000) and used to calculate the oxygen potential for the reactions using the following equation (R = gas constant, T = Temperature):

$$P_{O2} = e^{(\Delta G/RT)} \quad ...(XVI)$$

The activities of the solid phases were taken to be equal to one. The calculated results for the two reactions are shown in Figure 34. Figure 34 shows that over the range of temperatures applicable to this study, both reactions (N) and (O) are thermodynamically favorable in air ($\log P_{O2} = -0.68$). Based on this it is reasonable to expect that Fe_2TiO_5 and rutile would be the final phase assemblages at temperatures between 600 and 1000 °C. At lower temperatures the phase assemblages would be different, due to the decomposition of Fe_2TiO_5 (Haggerty and Lindsley, 1970).

Figure 34: The oxygen potential required for the oxidation of relevant M_3O_5 phases

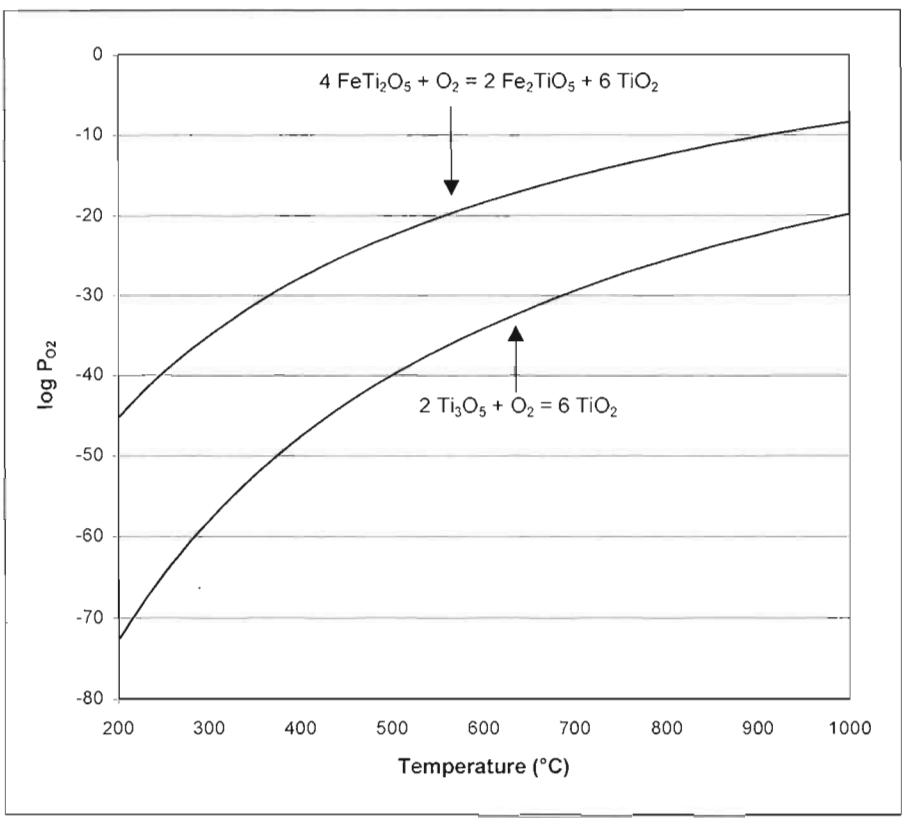

For the oxidation of titania slag at 650 °C (see suggested diagram, Figure 35) the following phase assemblages can be expected for increased oxidation of titania slag:

- Metallic iron, with a succession of two Magnéli phases up to rutile, when all the titanium will be oxidised to Ti^{4+} (various three phase regions). This is not indicated in the phase diagram, but assumed based on Figure 32.
- Metallic iron, with rutile and ilmenite (three phase region).
- Rutile and α-oxide (two phase region).

- Rutile, α-oxide (ilmenite) and spinel (three phase region).
- Rutile and spinel (two phase region).
- Rutile, α-oxide (iron-rich phase) and spinel (three phase region).
- Rutile and α-oxide (two phase region).
- Rutile, α-oxide and pseudobrookite (three phase region).
- Rutile and pseudobrookite (two phase region). Once again by increasing the extent of oxidation of the sample the amount of rutile relative to the amount of pseudobrookite increases. At the same time the amount of Fe^{3+} relative to Fe^{2+} also increases.
- The final phase assemblage will be rutile and Fe_2TiO_5, with all the iron oxidised to Fe^{3+}.

Figure 35 : Suggested phase diagram for the Fe-Fe_2O_3-TiO_2 system at approximately 650 °C. Compositions are in mol-units (from Borowiec and Rosenqvist, 1981)

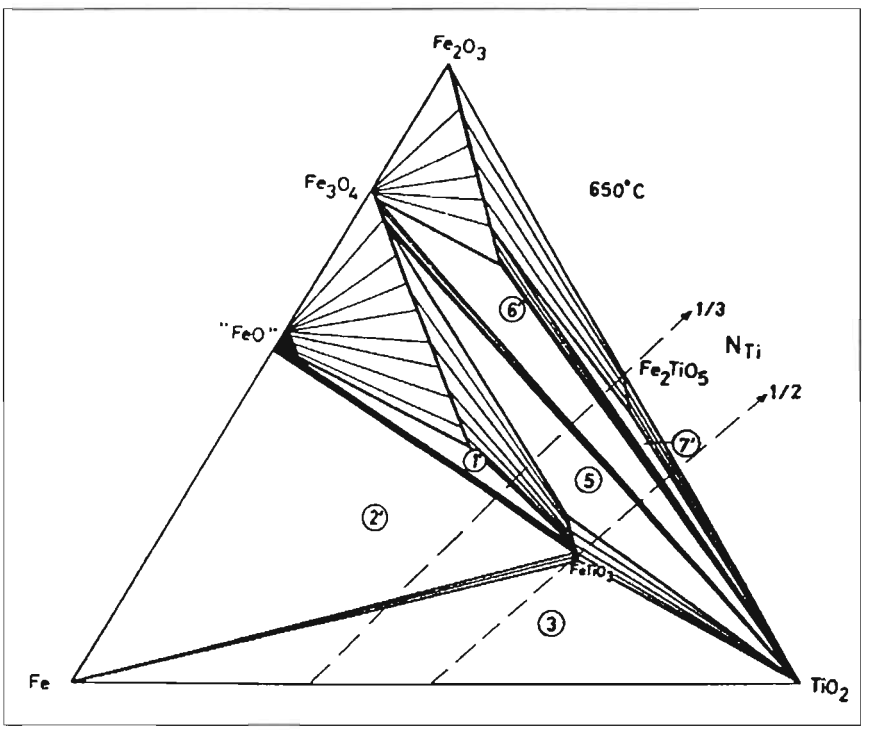

Gupta et. al. (1989) studied the phase relations in the Fe-Fe_2O_3-TiO_2 system at 700 and 900 °C, using a technique similar to that of Borowiec and Rosenqvist (1981). Their proposed isothermal phase diagram at 700 °C is shown in Figure 36. According to the results obtained by Gupta et. al. (1989) the spinel-rutile phase combination in the Fe-Fe_2O_3-TiO_2 system is not stable at 700 °C, explaining the differences between their phase diagram and that of Borowiec and Rosenqvist (1981) as shown in Figure 33. Despite these differences, the fully oxidised condition is given as TiO_2 + Fe_2TiO_5 in both cases.

The phase relations in the Ti_3O_5-Fe_2TiO_5 system as compiled by Borowiec and Rosenqvist (1985) as a function of temperature is shown in Figure 37. This diagram shows that for oxidised pseudobrookite (containing no or little Ti^{3+}), M_2O_3 and TiO_2 are the final phases at equilibrium at low temperatures (below 585 °C). Thus the final oxidation product changes from TiO_2 + Fe_2TiO_5 to TiO_2 + α-oxide at lower temperatures.

Figure 36: Proposed Fe-Fe_2O_3-TiO_2 phase diagram at 700 °C (Gupta et. al., 1989)

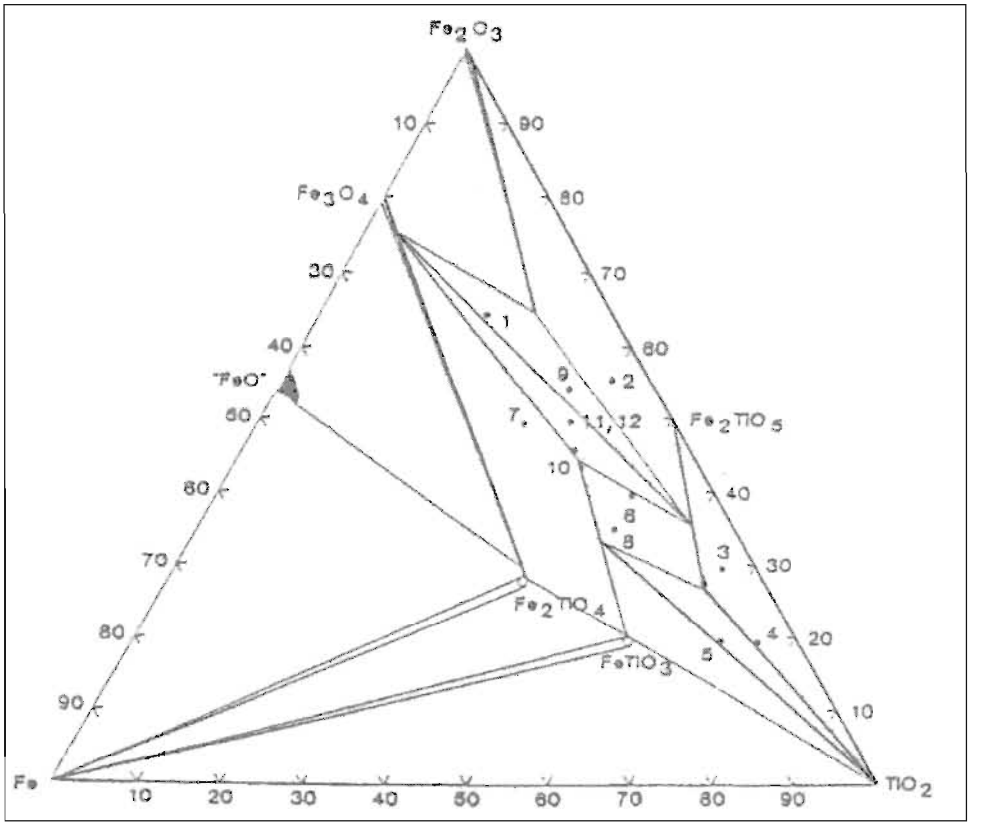

Figure 37: The Ti_3O_5-Fe_2TiO_5 system as a function of temperature (from Borowiec and Rosenqvist, 1985)

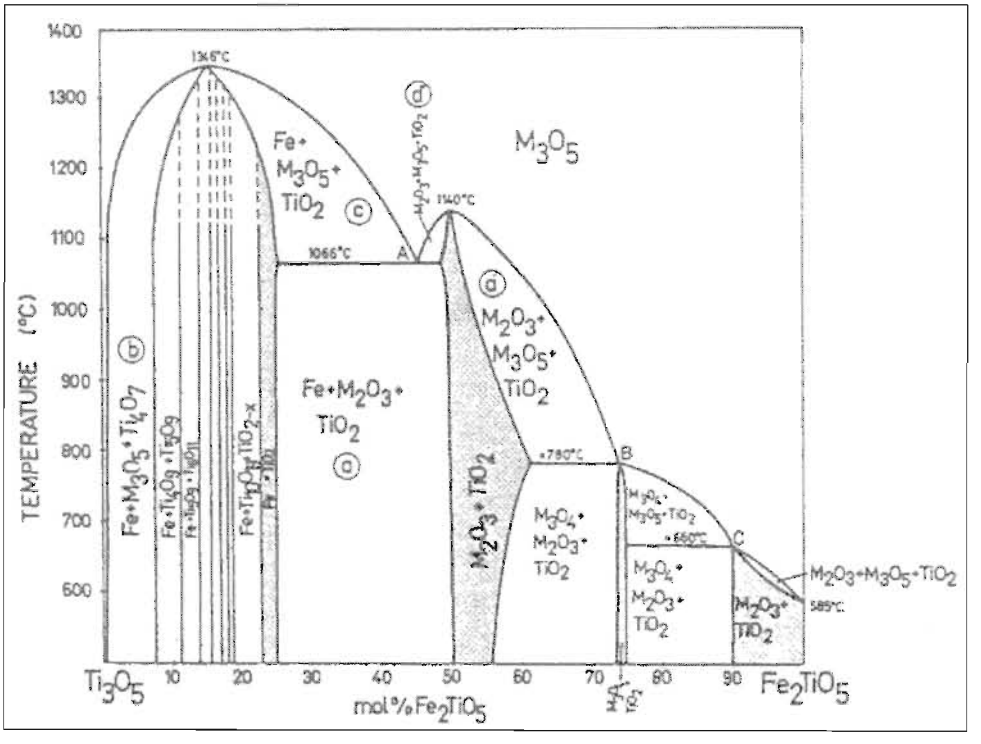

3.3 APPROACH FOR THE STUDY OF DECREPITATION OF TITANIA SLAGS

Based on the available information there are several possible ways in which high titania slags can decrepitate. The following possible reasons for the decrepitation of high titania slags were identified:

a) The formation of a new phase with a higher or lower molar volume. New phases can form by decomposition, or by oxidation. The mineralogical properties of various iron and titanium phases that could potentially exist in the system under investigation are shown in Table 22. Also included in Table 22 are the molar volumes of the various phases, indicating the magnitude of potential volume changes.
b) Polymorphic phase changes of some of the phases already present during cooling.
c) Differences in the coefficients of expansion of the metallic iron and the slag, with the metallic iron formed according to reaction (K). It is also possible that decrepitation of the slag can occur due to differences in the coefficients of expansion of other phases present in the slag.
d) Hydration of selected phases present in the slag. As no hydrated phases were previously observed in high titania slags it was however not considered to be a viable option.
e) Thermal shock of the slag on cooling was also considered as an option for decrepitation of the slag. However, as large blocks are cooled over extended periods of several days or weeks (depending on the size of the block) this was considered unlikely.

To test the various possibilities, high titania slag samples produced during various smelting campaigns in a pilot plant furnace (direct current configuration with a electrical rating of 1.5 MW) were obtained. These samples were then exposed to air under isothermal conditions in an effort to simulate the cooling process at various temperatures. Experiments were carried out between 400 and 1000 °C, as this seemed to be the temperature regime where decrepitation could be expected, both from the literature information and from observations of slag blocks produced at Iscor's pilot plant furnace. The data from these experiments were then compared with information gathered from decrepitated slags obtained during the cooling of large blocks (approximately one ton in size).

3.4 EXPERIMENTAL DETAILS

3.4.1 SLAG SAMPLES USED FOR SMALL-SCALE EXPERIMENTS

Several slag samples were used for the small-scale testwork. The chemical analyses of these samples are shown in Table 23.

3.4.2 TESTWORK ON PRESSED PELLET SAMPLES

3.4.2.1 Preliminary testwork on pressed pellets

As no prior information was available on the oxidation of titania slags to observe decrepitation behaviour, some initial experiments were carried out under a range of

experimental conditions in an attempt to observe the desired decrepitation behaviour and determine the best range of experimental conditions.

Slag DB91 was used as starting material for the preliminary tests (see Table 23 for composition). The slag was milled to a powder prior to use. For each test a pellet (15 mm in diameter) was pressed. The densities of the pellets were calculated using the dimensions of the pellets and the mass of each pellet. Alumina crucibles were used as sample holders. The pellets were placed in a Gallenkamp muffle furnace with silicon carbide elements situated in the roof. All the experiments were carried out in a stagnant air atmosphere. At the completion of each test the pellet was quenched in water. Some of the pellets completely disintegrated into a powder upon quenching, while for other experiments no change to the shape of the pellet was observed. The experimental details of the various preliminary tests are shown in Table 24. It was decided that the pellets for this program would be pressed at 817 atmospheres to obtain the maximum pellet density, using a total of 5.00 g of slag for each pellet.

3.4.2.2 Isothermal testwork on pressed pellets

Based on the results obtained on the preliminary work a detailed test program was drawn up to investigate the decrepitation behaviour of the titania slags, as well as the phase relations present in the samples. Slag DB100 (see Table 23) was used for this test program. The slag was milled to a d_{50} of 121 µm prior to use. Pellets were then pressed for this powder as described earlier. Experiments at 800 and 1000 °C were carried out in the Gallenkamp muffle furnace as described above. Experiments at lower temperatures were carried out in a Carbolite muffle furnace, also in a static air atmosphere. Alumina crucibles were used as sample holders in all instances. For each experiment the furnace was heated to the required temperature before inserting the sample in the furnace. The sample was then kept in the furnace for the required time. At the completion of the experiment the sample was removed from the furnace and quenched in water. On quenching some samples decrepitated to powder, while other samples retained their shape with some surface decrepitation. In some cases no signs of any decrepitation was observed. The samples were then dried at approximately 100 °C.

Temperatures inside the furnaces were verified by using a digital FLUKE multimeter and type K thermocouple probe. The equipment was calibrated as a system from 200 to 1000 °C by a South African National Accreditation System approved laboratory (Laboratory no. 308) using the procedure TEMP 08. The uncertainty of measurement was as follows:

- ± 2 °C for temperatures below 700 °C.
- ± 4 °C for temperatures above 700 °C.

Furnace temperatures were controlled to ± 10 °C of the setpoint temperature.

3.4.3 TESTWORK WITH MINIATURE SLAG BLOCKS

3.4.3.1 Isothermal testwork on miniature slag blocks

It was decided to compare the results obtained with the pressed pellets with those of solid pieces of slag. For this purpose a large solid piece of slag was cut with a diamond coated saw

Table 23 : Analyses of slag samples used for small-scale testwork

Slag no.	Analyses no.	Analyses (mass %)												
		SiO_2	Al_2O_3	CaO	MgO	MnO	Cr_2O_3	V_2O_5	ZrO_2	Fe^0	FeO	TiO_2	Ti_2O_3	Total Ti as TiO_2
7195	DB91	1.05	0.87	0.22	0.95	1.14	0.06	0.48	0.20	< 0.1	10.96	56.32	28.20	87.66
7030	DB100	1.41	1.19	0.27	1.03	1.17	0.05	0.45	0.16	< 0.1	9.80	53.9	30.4	87.70
7036	DB123	3.79	0.89	0.57	0.72	2.02	0.08	0.25	0.42	0.4	14.4	60.6	15.4	77.75
7051	DB136	1.50	0.96	0.25	1.22	1.11	0.05	0.46	0.16	0.13	8.40	52.04	33.92	89.74

Table 24 : Experimental details of the preliminary testwork

Test no.	Mass of pellet (g)	Pressure applied to form pellet (atmospheres)	Temperature (°C)	Time of test (hours)	Density of pellet ($g.cm^{-3}$)	Decrepitation observed
1	5.00	408	1000	46	2.83	No
2	5.00	408	500	71	2.83	Yes
3	5.00	817	750	101	2.99	No
4	4.00	817	750	101	2.96	No
5	5.00	817	350	98	-	Yes

to obtain miniature slag blocks. The blocks were cut in the approximate shape of a cube, with the length of each side ranging between 10 and 13 mm. Based on the mass, and the measured dimensions of nine of these blocks, the average apparent density was calculated to be 3.48 $g.cm^{-3}$ (standard deviation = 0.21). The analysis of the slag is shown in Table 23 (sample DB123). Unfortunately it was found after completion of these tests that the chemical analysis of the miniature slag blocks differed significantly from the slag used for the pressed pellet testwork (believed to be due to mistaken sample identification).

Testwork on the miniature slag blocks was carried out using the same methodology as previously described for the pressed pellet samples.

3.4.3.2 Unidirectional crushing tests on miniature slag blocks

The miniature slag blocks were made as described in the previous section, and were similar in their dimensions. Chemical analysis of these blocks is shown in Table 23 (slag DB136). The blocks were heated at various temperatures (400, 600 and 800 °C) and times (24 and 96 hours) in a muffle furnace. All the experiments were carried out as previously in air. At the completion of the experiments the samples were quenched in water, then dried at approximately 100 °C. All the samples treated at 400 °C decrepitated completely on quenching, with the remainder of the samples retaining their cubic shape.

Both treated and untreated miniature slag blocks were then subjected to unidirectional compression strength tests using a Monsanto Tensometer. A simplified schematic of the equipment used for the unidirectional compression strength testwork is shown in Figure 38. The blocks were fixed to the moving plate with elastic bands. The elastic passed on the side of the blocks, so that the initial contact of the block surface was directly with the fixed plate. With each experiment the plate with the block was moved towards the fixed plate by means of an electric motor at a rate of approximately 6 $mm.s^{-1}$ prior to the sample coming in contact with the fixed plate. After the sample made contact with the fixed plate this rate decreased markedly due to elastic deformation of the testing apparatus. This is discussed in more detail in section 3.5.2.2. The moving plate was stopped approximately 2 mm from the fixed plate using a limit switch. Data on the position of the moving plate and the applied force was collected as a function of time. The data output for the position of the miniature slag block and force applied to the block was recorded as volts, while the time output was in seconds. It was therefore necessary to calibrate the equipment for each series of tests to obtain conversion constants to convert the position and applied force readings to millimeter and kilo-newton respectively. Two series of tests were carried out, consisting of eight tests in each series.

3.4.4 TESTWORK ON THE EFFECT OF DIFFERENT ATMOSPHERES ON DECREPITATION

In order to test the effect of an inert atmosphere on decrepitation several tests were carried out. For this purpose powder samples from sample DB100 (see Table 23 for composition) were used. The experiments were carried out in a vertical silica tube reactor at 370 and 400 °C. The reactor was heated to the required temperature in either argon or air. After the temperature was attained the sample (~ 10 g) was introduced. The samples were heated for periods between 24 and 72 hours. Several experiments were carried out in argon before a leak

in the system was discovered through partial oxidation of these samples. It was still possible to extract some useful information from these tests (discussed later). After repairing the leak another test in argon was completed successfully.

Figure 38: Simplified schematic of the equipment used for the unidirectional crushing tests

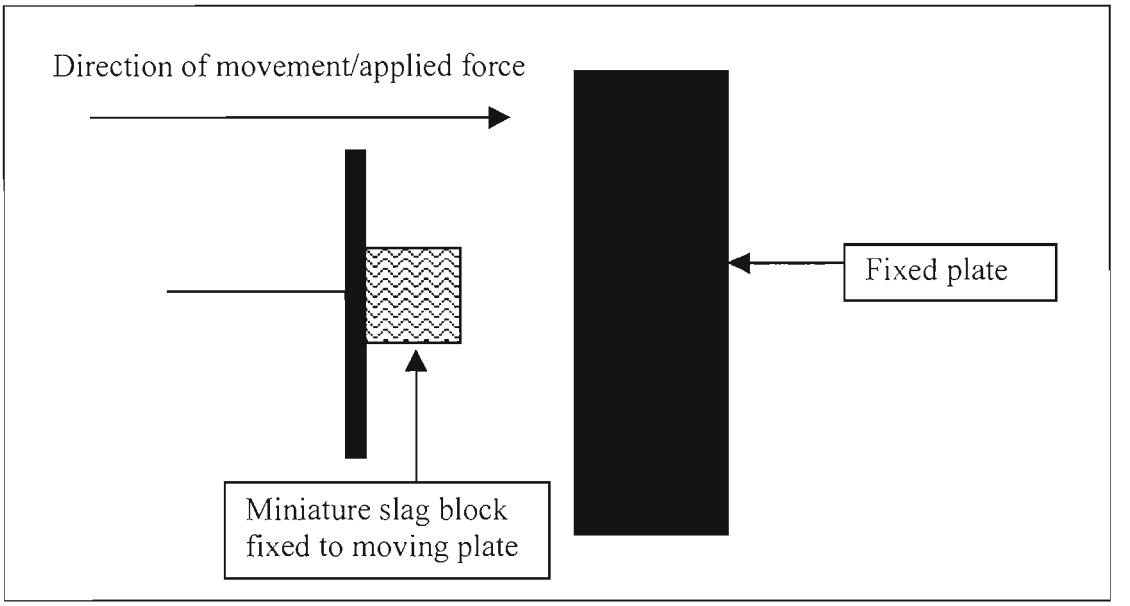

3.4.5 TESTWORK CARRIED OUT DURING THE PILOT PLANT ILMENITE SMELTING CAMPAIGN

3.4.5.1 Determination of the cooling rate of the slag blocks

Ilmenite was smelted in the Iscor pilot plant furnace (direct current configuration; rated at 1.5 MW) to produce titania slag. The slag was tapped at regular intervals, with the approximate tap sizes being one ton. The cooling rates of two of these slag blocks (tap numbers 73 and 79) were measured. This was done by inserting a thermocouple assemblage inside the slag block directly after tapping, and measuring the temperature inside the slag block until a temperature of less than 200 °C was attained. After tapping the slag into the ladle, a channel iron frame (in the shape of a +) was placed across the ladle in which the slag was tapped. This frame had a hole in the center through which the thermocouple assemblage was inserted. For tap 73 the thermocouple assemblage was inserted into the slag approximately four minutes after the taphole was closed, while for tap 79 the thermocouple assemblage was inserted approximately one minute after the taphole was closed. Temperature readings were taken at regular intervals by using a multimeter device. The slag blocks remained in the ladles until the measurements were completed.

The thermocouple assemblage was made up of three different sheaths, placed inside each other. The smallest sheath housed a type S thermocouple. The dimensions of the sheaths were as follows:

- External SiC sheath

  - 600 mm length
  - 44 mm outer diameter (OD)
  - 25 mm inner diameter (ID)
- Outer Alumina sheath
  - Approximately 610 mm in length
  - 17 mm OD
  - 12 mm ID
- Inner Alumina sheath
  - Approximately 620 mm in length
  - 10 mm OD
  - 6 mm ID

The thermocouple assemblage was made in this way, as there was some concern about a single sheath protecting the thermocouple for the duration of the measurements. This concern was however unfounded, as the SiC sheath was found to be intact in both instances after completion of the measurements.

3.4.5.2 Decrepitated slag samples

Decrepitated slag samples were collected from two slag blocks. As the slag blocks decrepitated, small heaps of decrepitated material formed adjacent to the blocks. Grab samples were taken from these heaps over a period of time.

3.4.6 ANALYTICAL TECHNIQUES

The analytical techniques used in the study of the decrepitation of the titania slags were the same that was used as described previously. Elemental phase analyses of various samples are again given in Appendix B.

X-ray diffraction analyses of the oxidised products produced in this section proved to be challenging, as several of the products produced contained overlapping peaks making phase identification difficult. This is particularly so at a d value of approximately 3.50 Å. The approximate d-values shown in Table 25 were used for the identification of the various phases. The d-values (and therefore also the 2θ-values) were slightly shifted for some samples in the accumulation of the patterns. The following explanations are possible in explaining these shifts:

- Displacement of the sample (samples were placed on glass plates) from the focussing circle of the diffractometer (Schreiner and Jenkins, 1982).
- The zero position of the instrument. This can however be excluded as the instrument was calibrated.
- Small changes in the structure of the solid solution phases due to the experimental treatments.

The relationship between the d-values and the 2θ values is given by the well-known Bragg equation:

$$n\lambda = 2d\sin\theta \quad \ldots(XVII)$$

In this study the wavelength (λ) used was that of Cu, at 1.54056 Å. The X-ray diffraction patterns for the relevant samples in this section are given in various Appendices.

Table 25: Peak positions used for phase identification

Phase	d-values (Å)	2θ values
M_3O_5	3.48, 2.75	25.6, 32.5
Ilmenite	3.73, 2.53, 1.72	23.8, 35.5, 53.2
Rutile	3.25	27.4
Anatase	3.52, 2.38, 1.89, 1.70, 1.67	25.3, 37.8, 48.1, 54.0, 55.1
Hematite	2.69	33.3
M_6O_{11}	4.20, 3.50, 2.46, 1.87	21.1, 25.5, 36.5, 48.6

3.5 RESULTS AND DISCUSSION

It is important to make a comment with regard to the Mössbauer results for the samples treated at temperatures of 600 °C and lower. For these samples the Mössbauer data was interpreted as still containing iron in the pseudobrookite (M_3O_5) phase. As will be discussed later, it was however found that changes in the M_3O_5 structure occurred. It is however likely that iron in the changed structure still occupies octahedral sites. This will however need to be confirmed. In the various tables containing the Mössbauer results, the attribution of iron is therefore still indicated as being pseudobrookite. It should however be remembered that this is not a "true pseudobrookite", but a transformed M_3O_5 product. One of the consequences of this might be that the oxidation states inferred from the Mössbauer data are incorrect, or that the errors in the data might be larger.

This is one of the reasons why the oxidation states for specific phases in samples treated at 600 °C and lower were not calculated, as some anomalous results were obtained. The second reason for not calculating the oxidation states for these samples are due to the uncertainty of the oxygen analysis as discussed earlier (see section 2.3.2.1).

3.5.1 RESULTS OBTAINED FROM THE PRESSED PELLET SAMPLES

Sample DB100 was used as starting material for the testwork on the pellet samples. The chemical composition of this sample is shown in Table 23. X-ray diffraction patterns for these samples are given in Appendix G.

3.5.1.1 Results of testwork at 1000 °C

Experiments were carried out at 1000 °C for periods of 24 and 384 hours (samples DB104 and DB106 respectively). All the samples treated at 1000 °C contained slag particles that were porous. This can be seen quite clearly in Figure 39, for the sample heated for 24 hours.

The slag particles in all the samples consisted of a mixture of rutile (dark colour) and M_3O_5 (light colour) phases. This phase assemblage is predicted by the phase diagram obtained by Borowiec and Rosenqvist (1981) at 950 °C. These phases were identified by X-ray diffraction

analyses, with rutile being the major phase present. Mössbauer analyses of the sample treated for 24 hours (sample DB104; see Table 26) indicate the presence of metallic iron and a pseudobrookite (M_3O_5) phase. These products probably formed by disproportionation (reaction (K)) as suggested by Toromanoff and Habashi (1984).

Figure 39: Photograph of a pellet sample treated at 1000 °C for 24 hours (Sample no. DB104)

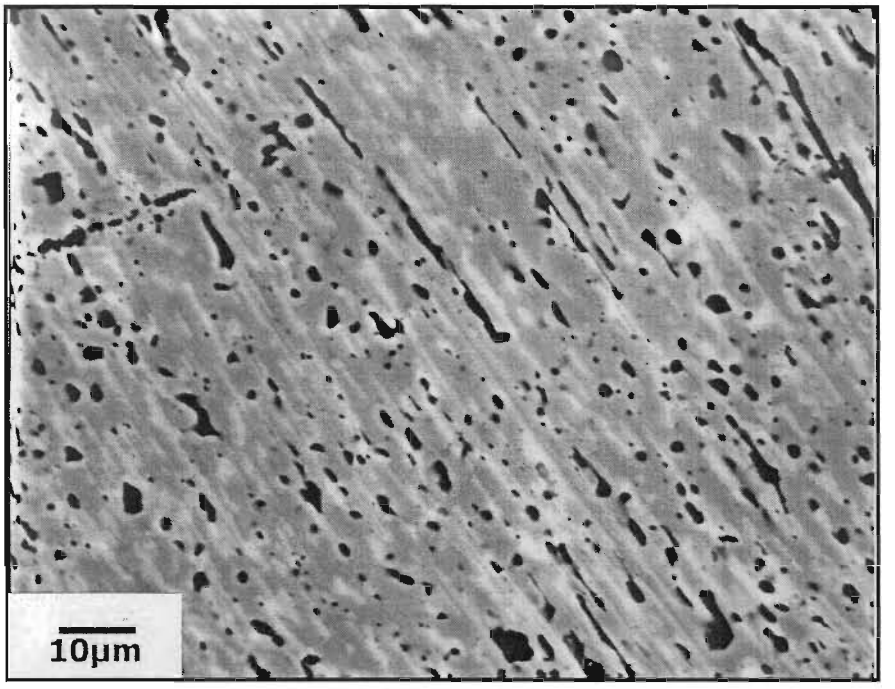

The pseudobrookite phase only contained Fe^{3+}, indicating that this phase was fully oxidised. This was found for both the samples treated at 1000 °C (24 and 384 hours). It seems from the Mössbauer results that the sample treated for 384 hours (DB106) might contain an additional hematite-like phase. This is however not certain, due to the high relative error obtained (the error is equal to the iron abundance). It can be speculated that if the hematite-like phase is present, it could possibly be due to some of the metallic iron being oxidised to hematite.

No decrepitation of these two samples was observed.

3.5.1.2 Results of the testwork at 800 °C

A photograph of the sample treated for 24 hours (DB109) is shown in Figure 40. The slag particles are shown to be finely porous, with the majority of the particles displaying well-defined, iron-enriched outer rims. Rutile and the M_3O_5 solid solution series phase were identified by X-ray diffraction analysis, with these phases intimately mixed together. This is in line with the phase diagram (see Figure 32). It is probable that some anatase is also present, although this could not be confirmed with absolute certainty using X-ray diffraction. From the Mössbauer spectroscopy results shown in Table 26 a hematite-like phase (written as M_2O_3) and metallic iron phase were also identified. The concentrations of these phases were however too low to be identified by X-ray diffraction analysis.

Table 26: Summary of results obtained from Mössbauer spectroscopy for the pressed pellet samples heated at 800 and 1000 °C

Sample no.	Temperature (°C)	Time (hours)	Hyperfine interaction parameters			Abundance (atom %)	Attribution
			Isomeric shift - δ ($mm.s^{-1}$)	Quadropole splitting - Δ ($mm.s^{-1}$)	B_{hf} (T)		
DB100	Starting slag		1.16 (2)	3.35 (4)	-	90 (2)	Fe^{2+} compound (ferropseudobrookite)
			1.09 (2)	1.83 (4)	-	10 (2)	
DB104	1000	24	0.39 (5)	0.75 (4)	-	73 (2)	Fe^{3+} compound (pseudobrookite)
			0.00 (2)	0.014 (4)	33	27 (2)	Metallic iron
DB106	1000	384	0.38 (2)	0.76 (2)	-	84 (2)	Fe^{3+} compound (pseudobrookite)
			0.00	-0.078	32.9	14 (2)	Metallic iron
			0.51 (3)	-0.91 (3)	49.6 (1)	2 (2)	Hematite-like compound (Fe^{3+})
DB109	800	24	0.38 (2)	0.74 (5)	-	69 (2)	Fe^{3+} compound (pseudobrookite)
			0.02 (2)	-0.01 (3)	33.0 (1)	20 (2)	Metallic Fe
			0.36 (2)	-0.12 (5)	50.3 (2)	11 (2)	Hematite-like compound (Fe^{3+})
DB105	800	384	0.38 (2)	0.75 (5)	-	80 (2)	Fe^{3+} compound (pseudobrookite)
			0.116(2)	-0.08 (3)	32.9 (1)	13 (2)	Metallic iron
			0.46 (2)	-0.18 (5)	50.4 (2)	11 (2)	Hematite-like compound (Fe^{3+})

Errors are quoted as percentage (in parenthesis)
B_{hf} – internal magnetic field

The iron present in the M_2O_3 phase was identified as being trivalent by the Mössbauer spectroscopy results. Once again only the presence of Fe^{3+} and Fe^0 are indicated. The presence of metallic iron is once again believed to be due to reaction (K) as mentioned previously.

Figure 40: Photograph of a pellet sample treated at 800 °C for 24 hours (sample DB109)

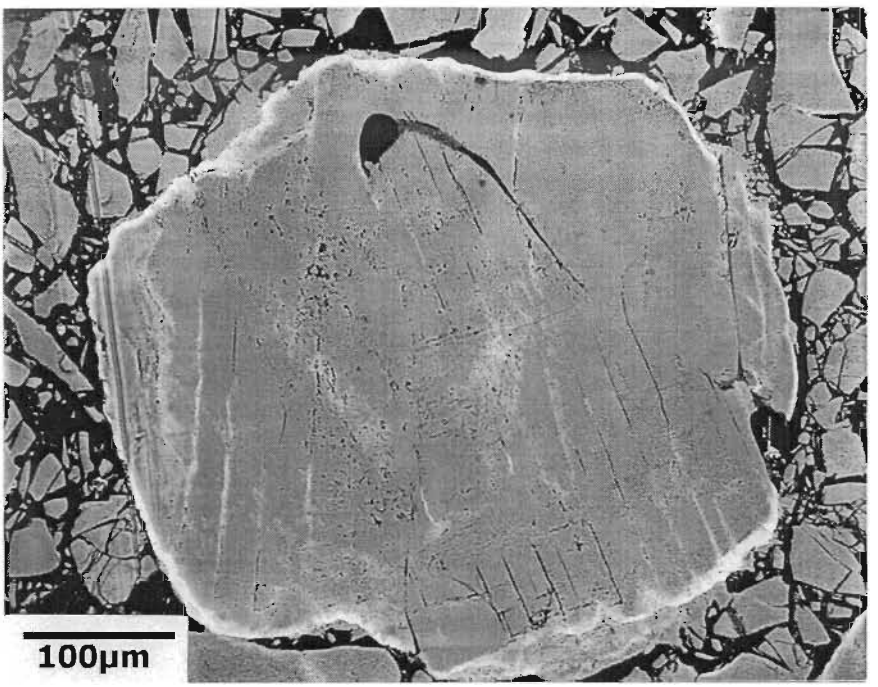

For a sample treated at 384 hours (DB105) both rutile and the M_3O_5 phase were identified by X-ray diffraction. It is however noticeable that the X-ray diffraction pattern (Appendix G) had become indicative of a more amorphous structure compared to sample DB109, indicating increasing disorder in the crystal structure of the phases. Metallic iron and M_2O_3 phases were also identified using Mössbauer spectroscopy (see Table 26). A photograph of this sample is shown in Figure 41. The slag particles in this sample appear to be more porous compared to the sample treated for 24 hours. This sample also displays a well-defined iron enriched outer rim. A phase analysis of the rim showed a M/O molar ratio of 0.66, as expected for the α-oxide (M_2O_3). The chemical composition of the rim phase was calculated to be as follows:

$$Fe^{2+}_{0.38}\,Fe^{3+}_{1.14}\,Al^{3+}_{0.02}\,Mn^{2+}_{0.02}\,Mg^{2+}_{0.02}\,Ti^{4+}_{0.42}\,O^{2-}_{3}$$

The oxidation state of iron was calculated by assuming a charge balance, as well as assuming the oxidation states of the other cations as indicated. It was assumed that only Fe^{2+} and Fe^{3+} are present, with the composition of the phase showing that it is essentially a M_2O_3 solid solution. However, according to the Mössbauer results the hematite-like phase only contained Fe^{3+}. If this is correct, it implies that there must be some Ti^{3+} present in order to maintain the charge balance. This scenario is considered most unlikely. From the composition and charge balance it does seem more likely that some Fe^{2+} is present. The end members of the solid solution are Fe_2O_3 (iron as Fe^{3+}) and $FeTiO_3$ (iron as Fe^{2+}). At 800 °C this solid solution is still continuous (see Figure 32). The composition of the rim phase is closer to the hematite

end member. This is illustrated by taking the solid solution end members into account, and re-writing the composition of the rim phase as follows:

$$0.42\left[\left(Fe_{0.90}^{2+}Mn_{0.05}^{2+}Mg_{0.05}^{2+}Ti_{1.00}^{4+}\right)O_{3}^{2-}\right]\bullet 0.01\left[Al_{2}^{3+}O_{3}^{2-}\right]\bullet 0.57\left[Fe_{2}^{3+}O_{3}^{2-}\right]$$

Figure 41: Photograph of a pellet sample treated at 800 °C for 384 hours (sample DB105)

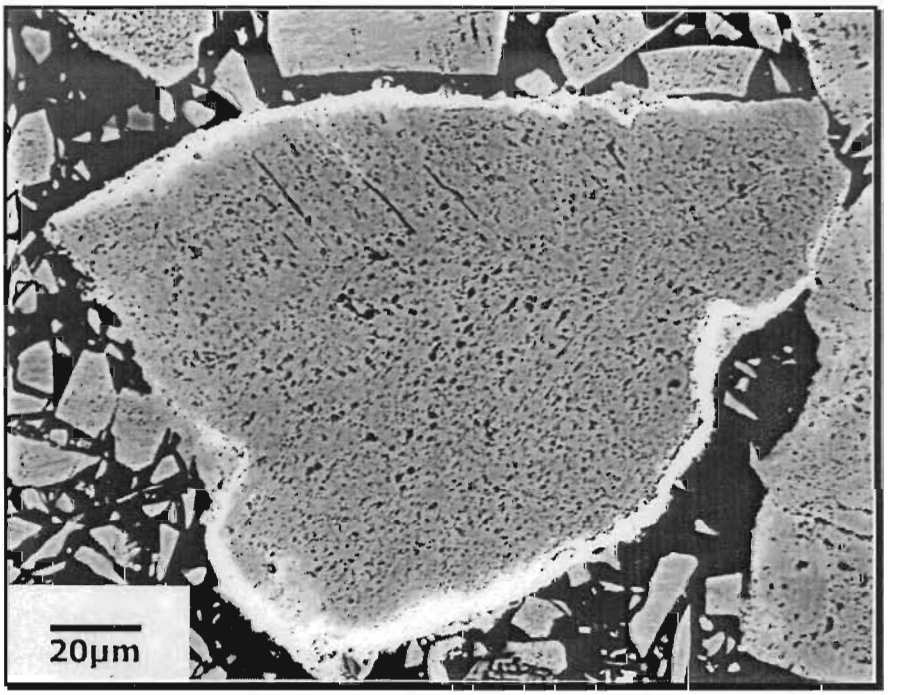

According to the phase diagram in Figure 32, the final phase assemblage at equilibrium at 800 °C should be TiO_2 (rutile) and Fe_2TiO_5 (pseudobrookite). This indicates that the rim is not in equilibrium with the core.

Of interest is the high level of porosity that is observed in the samples treated at the higher temperatures. This is illustrated for example in Figure 39 and Figure 41. Two possible reasons for this phenomenon are presented:

- A reduction in volume due to phase changes. Consider for example reaction (P) that could be expected to occur:

$$4FeTi_2O_5 + O_2 = 2Fe_2TiO_5 + 6TiO_2 \ldots(P)$$

  Using the data from Table 22 the starting volume for the reaction can be calculated to be 223.3 cm^3 (for 4 moles of $FeTi_2O_5$), while the finishing volume is calculated to be either 222.5 cm^3 (based on rutile) or 232.1 cm^3 (based on anatase). This result indicates only a marginal decrease (0.4 per cent) in the expected volume in the case of rutile, while in the instance of anatase being produced an increase (3.9 per cent) in the volume is calculated. Based on the X-ray diffraction results, rutile is the dominant phase in these samples. To create porosity in a sample a decrease in the volume is required. Therefore reaction (P) does not give an explanation for the observed porosity. A similar calculation was carried

out for the oxidation of Ti_3O_5 to TiO_2. This also resulted in an increase in the volume. Any inaccuracies of the data contained in Table 22 might however change the scenario. The effect of temperature (i.e. the thermal expansion coefficients) on the data in Table 22 might also change the results.

- Porosity could also develop due to the migration of cations (specifically iron) to the surface of the particles, thereby causing the development of pores in the interior of the particles. Such migrations were observed in some cases, with iron-rich rims observed in some samples (see for example Figure 41). This explanation seems more likely than the first one. This is however not a likely cause in the case of oxidation at 1000 °C where no iron-rich rim had formed.
- Another possibility is the contribution of short-range migration to porosity. The initial phase is a single, homogeneous phase (M_3O_5). Through a process of nucleation and growth, rutile and a second M_3O_5 phase is formed. The grain growth requires a diffusion process that can lead to porosity. This explanation will also account for porosity found at 1000 °C where no iron-rich rims had formed.

3.5.1.3 Results of the testwork at 600 °C

A photograph of the sample treated for 24 hours (DB115) is shown in Figure 42. The large slag particles in this sample display a zoned texture, with iron enriched outer margins, titanium-rich mantle zones and large cores with a dense and smooth appearance. An example of a large particle (approximately 400 µm by 550 µm in size) is shown in Figure 42. As mentioned previously, the d_{50} of the milled slag used for making the pellets is 121 µm. This indicates that these large particles are not representative of the sample used. Figure 43 shows the iron and titanium analyses (by WDS) from the centre of such a large particle to the rim of the particle. This figure illustrates the change in composition of iron and titanium over the three phases. Both rutile and anatase were clearly identified by X-ray diffraction analyses. Iron enrichment also occurs at the edges of the cracks. Fine metallic iron precipitates were also found to be present. The smaller particles (majority of the sample) were completely transformed to the titanium-rich phase, with iron-rich rims. Mössbauer data for this sample (Table 27) also shows the presence of a hematite-like phase. This was also confirmed by the X-ray diffraction analysis. It is interesting to note that the M_3O_5 peak at a 2θ-value of 32.5 degrees had almost completely disappeared, while the peak at a 2θ-value 25.5 degrees still showed the highest intensity. The ratio for these two peaks ($I_{2\theta=32.5}/I_{2\theta=25.5}$) for the starting material (DB100, see Appendix G) is 0.52, while for sample DB115 the ratio is 0.06. This difference can be explained by the near disappearance of the original M_3O_5 phase and the formation of anatase (main peak at a 2θ-value of 25.5 degrees).

The compositions of the various zones are given below. The typical composition of the core region was as follows, with a total of 3.07 cations obtained for every 5 oxygen atoms:

$$Fe_{0.21}Al_{0.05}V_{0.01}Mn_{0.01}Mg_{0.10}Ti_{2.69}O_5$$

A typical composition of the mantle zone is as follows (oxygen content normalised to 2):

$$Fe_{0.01}Al_{0.01}V_{0.01}Mg_{0.03}Ti_{1.01}O_2$$

There are a total of 1.07 cations for every 2 oxygen atoms.

Figure 42: Photograph of a pellet sample treated at 600 °C for 24 hours (sample DB115)

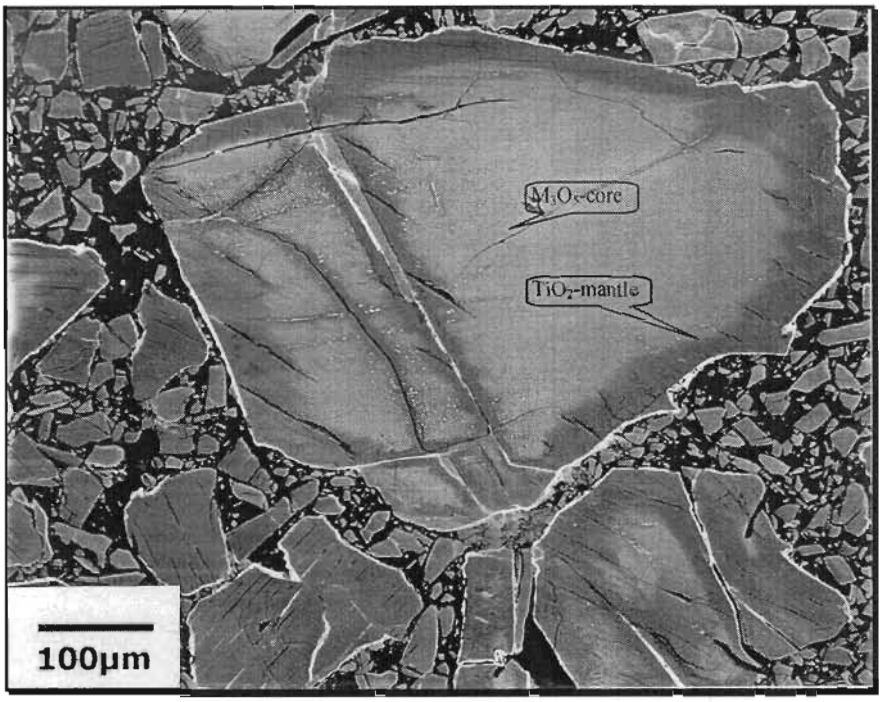

Figure 43: Iron and titanium analyses from the centre to the rim of a typical particle treated at 600 °C for 24 hours (sample DB115)

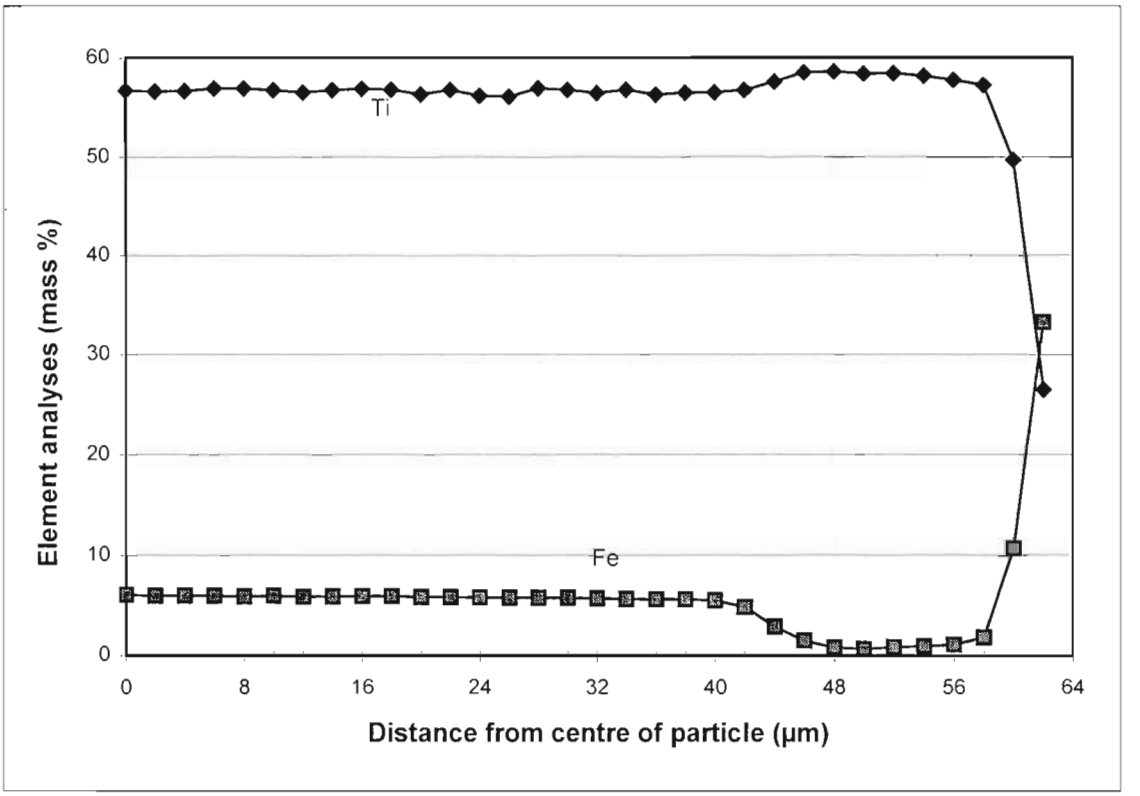

Table 27: Summary of results obtained from Mössbauer spectroscopy for the pressed pellet samples heated at 400 and 600 °C

Sample no.	Temperature (°C)	Time (hours)	Hyperfine interaction parameters			Abundance (atom %)	Attribution
			Isomeric shift - δ ($mm.s^{-1}$)	Quadropole splitting - Δ ($mm.s^{-1}$)	B_{hf} (T)		
DB100	Starting slag		1.16 (2)	3.35 (4)	-	90 (2)	Fe^{2+} compound (ferropseudobrookite)
			1.09 (2)	1.83 (4)	-	10 (2)	
DB115	600	24	0.39 (1)	0.66 (2)	-	47 (2)	Fe^{3+} compound (pseudobrookite)
			1.07 (1)	3.07 (4)	-	11 (2)	Fe^{2+} compound (ferropseudobrookite)
			0.38 (2)	-0.20 (2)	50.8 (2)	42 (2)	Hematite-like compound (Fe^{3+})
DB114	600	384	0.39 (2)	0.68 (2)	-	55 (2)	Fe^{3+} compound (pseudobrookite)
			0.38 (3)	-0.20 (3)	50.8 (1)	45 (2)	Hematite-like compound (Fe^{3+})
DB128	400	48	0.32 (1)	0.65 (2)	-	37 (2)	Fe^{3+} compound (pseudobrookite)
			1.09 (1)	3.07 (4)	-	43 (2)	Fe^{2+} compound (ferropseudobrookite)
			1.00 (2)	2.23 (2)	-	20 (2)	
DB125	400	384	0.39	0.68	-	55 (2)	Fe^{3+} compound (pseudobrookite)
			1.09	3.05	-	45 (2)	Fe^{2+} compound (ferropseudobrookite)

Errors are quoted as percentage (in parenthesis)
B_{hf} – internal magnetic field

A typical composition of the rim phase is as follows (oxygen content normalised to 3):

$$Fe_{1.64}Al_{0.06}Mn_{0.01}Mg_{0.02}Ti_{0.29}O_3$$

There are a total of 2.02 cations for every 3 oxygen atoms.

A photograph of the sample treated for 384 hours (DB114) is shown in Figure 44. The particles consist predominantly of the anatase and rutile as identified by X-ray diffraction analysis. As for sample DB115 the X-ray diffraction pattern also indicates that the M_3O_5 phase had almost disappeared. The slag particles are finely porous. According to the Mössbauer spectroscopy results shown in Table 27 a hematite-like compound (M_2O_3 phase) containing only Fe^{3+} was also identified. This was also confirmed by the X-ray diffraction results. This correlates with the iron-rich rims observed in Figure 44. The M_3O_5 phase (pseudobrookite) was also identified by Mössbauer spectroscopy, with this phase only containing Fe^{3+}.

Figure 44: Photograph of a pellet sample treated at 600 °C for 384 hours (sample DB114)

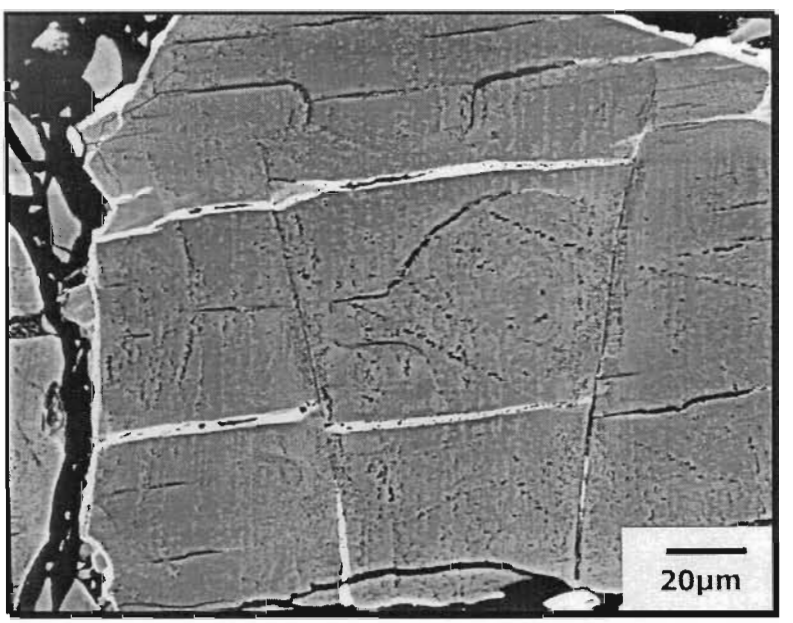

In general, only minor decrepitation of the samples treated at 600 °C was observed. This decrepitation occurred on the surface of the pellets, with the surface crumbling away.

3.5.1.4 Results of the testwork at 400 °C

All the samples treated at 400 °C decrepitated completely on quenching. This was also found for the sample treated for 2 hours (DB129). A photograph of a sample treated at 400 °C for 2 hours is shown in Figure 45. This photograph shows that extensive cracking of the particles had taken place when compared to the samples treated at 600 °C and higher temperatures. A sample treated for 96 hours is shown in Figure 46. The same type of cracks is observed in this sample, although the area density of the cracks seems to be slightly higher based on visual observation.

Figure 45: Photograph of a pellet sample treated at 400 °C for 2 hours (sample DB129)

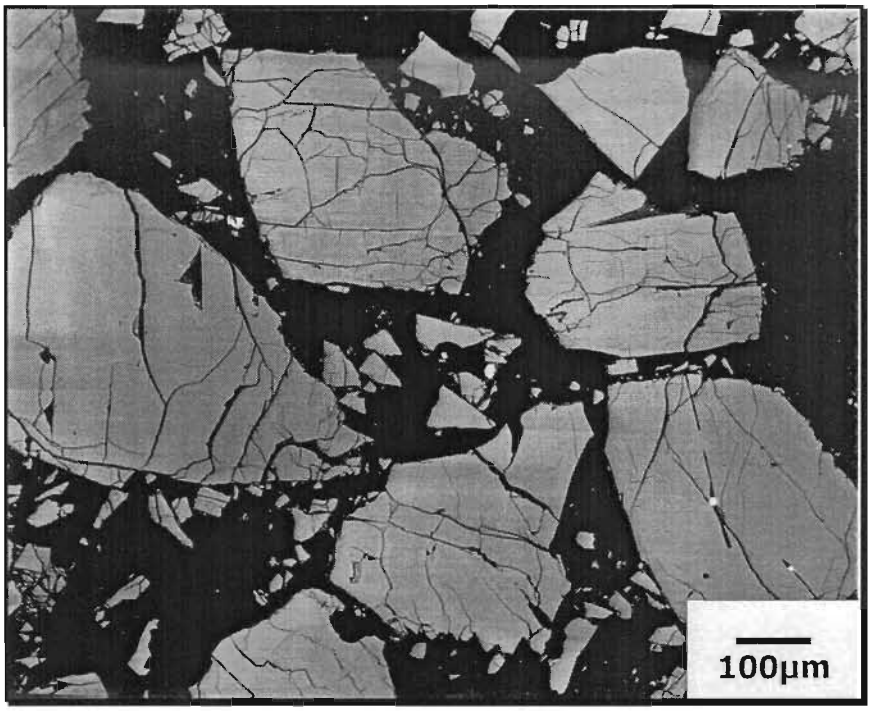

Figure 46: Photograph of a pellet sample treated at 400 °C for 96 hours (sample DB122)

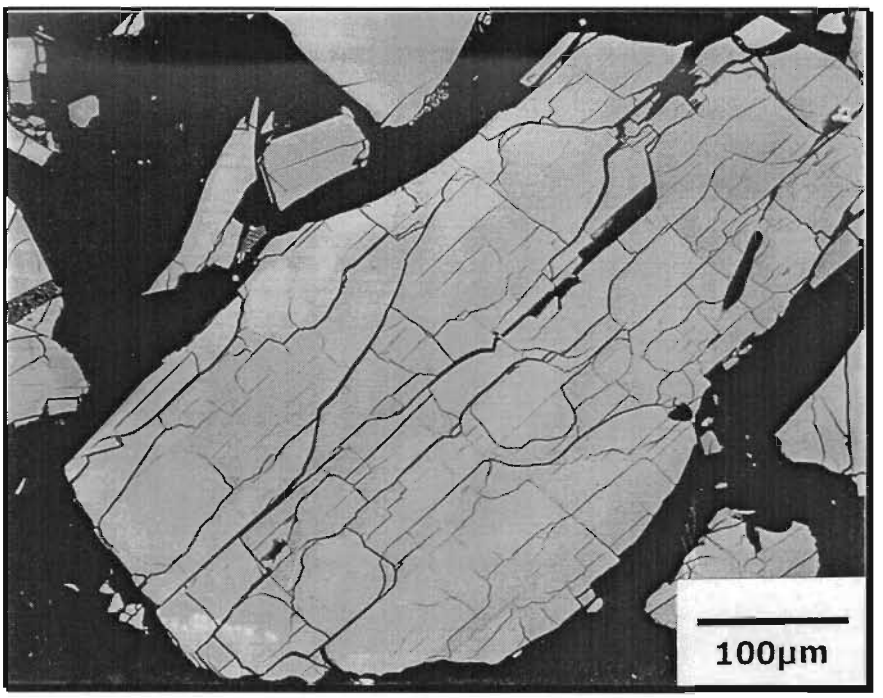

The X-ray diffraction patterns of some samples treated at 400 °C are also given in Appendix G. What is immediately noticeable is that the diffraction patterns show that the samples have became more amorphous when compared to the pattern for the starting material (DB100). This indicates increasing disorder in the crystal structure of the phases present. Also noticeable is the almost complete disappearance of the M_3O_5 peak at a 2θ-value of 32.5 degrees, whilst the peak at a 2θ-value of 25.3-25.6 degrees remains as the peak with the highest intensity. The results obtained for the various samples are summarised in Table 28, with the $I_{2\theta=32.5}/I_{2\theta=25.5}$ ratio also being plotted. The $I_{2\theta=32.5}/I_{2\theta=25.5}$ ratio is taken as an indication of the presence of the M_3O_5 phase. The results show that after 24 hours it seems that the M_3O_5 phase had almost completely disappeared. The question can then be asked what replaces the M_3O_5 phase?

Table 28: A summary of the relative peak intensities for the various samples treated at 400 °C for various times

Sample no.	Time (Hours)	2θ-value (degrees)	Intensity of the peak at a 2θ-value of ~ 25.5 degrees	2θ-value (degrees)	Intensity of the peak at a 2θ-value of ~ 32.5 degrees	$I_{2\theta=32.5}/I_{2\theta=25.5}$
DB100	0	25.6	3021.6	32.8	1564.7	0.518
DB129	2	25.6	896.4	32.7	262.5	0.293
DB121	24	25.6	753.2	32.3	57.0	0.076
DB128	48	25.7	1659.0	32.7	149.0	0.090
DB125	384	25.7	1462.6	32.9	102.6	0.070

Also noticeable is the appearance of a broad peak at a 2θ-value of approximately 21.1 degrees. This is similar to the peak obtained by Grey, Cranswick, et. al. (2000) as shown in Figure 31 for $Mg_{0.3}Ti_{2.7}O_5$ oxidised at low temperatures. Rietveld refinement of the M_6O_{11} intergrowth phase by Grey, Cranswick, et. al. (2000) show that the two major peaks for the M_6O_{11} phase are present at 2θ-values of 25.5 and 48.6 degrees respectively. At a 2θ-value of approximately 21.1 degrees some of the lesser peaks are also present. The position of these peaks correlates reasonably well with the data obtained for the samples treated at 400 °C. It can therefore be postulated that the disappearance of the M_3O_5 phase in the samples treated at 400 °C can be explained by the M_3O_5 phase being transformed into a M_6O_{11} phase. It seems that small amounts of anatase are also present in the oxidised pellet samples. This was also found by Grey, Cranswick, et. al. (2000) in their samples.

Mössbauer spectroscopy data of selected samples treated at 400 °C are shown in Table 27. These results show that a significant portion of the iron content is still in the +2 oxidation state. This is so even for the sample treated at 384 hours, indicating the slow rate of oxidation.

From point analysis of the bulk phase for the sample treated at 384 hours (Sample DB125, point a in Figure 47) the following compositions was calculated (oxygen content normalised to 5):

$$Fe_{0.22}Al_{0.04}V_{0.01}Mn_{0.01}Mg_{0.05}Ti_{2.50}O_5$$

Figure 47: Photograph of sample treated at 400 °C for 384 hours (DB125)

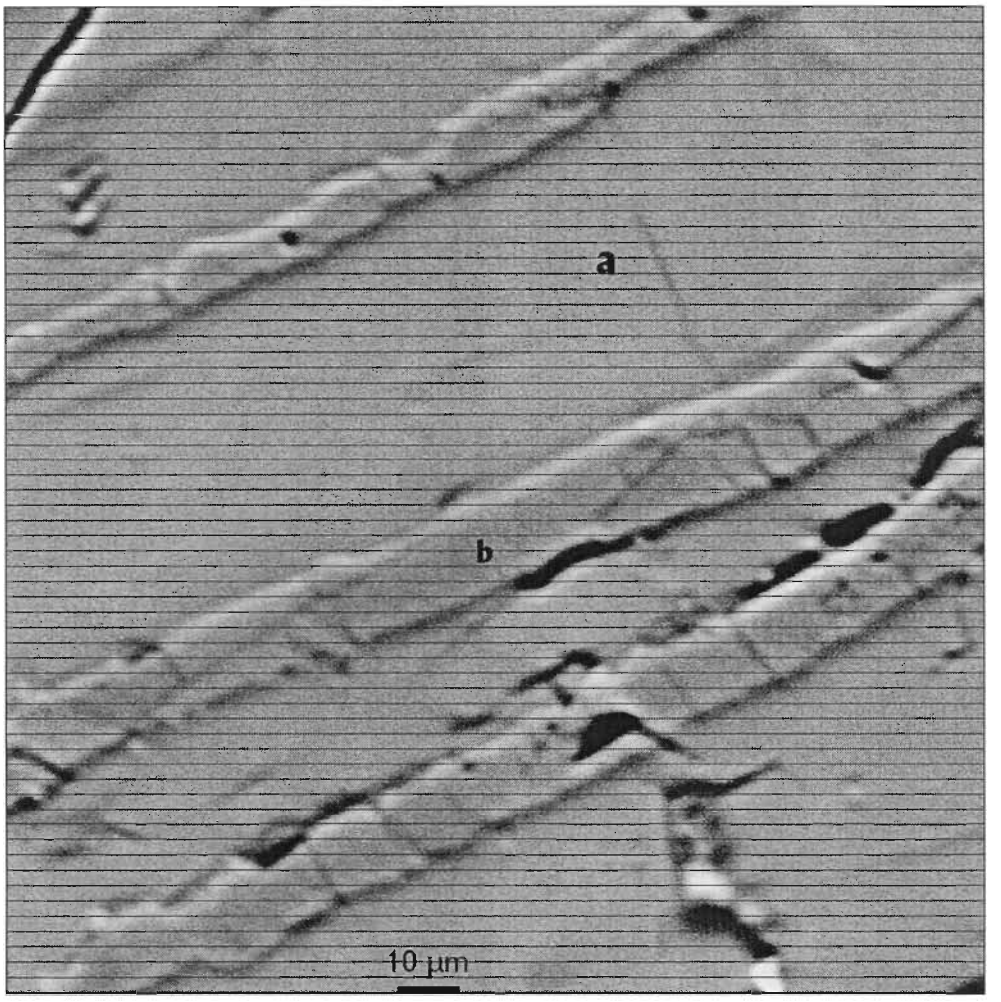

There are a total of 2.83 cations for every 5 oxygen atoms. When compared to the starting material (DB100) it can be seen that the oxygen to cation ratio of the bulk phase had increased. The X-ray diffraction pattern of the sample however shows almost none of a M_3O_5 phase to be present, and the cation to oxygen ratio is lower than can be expected for a M_3O_5 phase. As discussed previously it was not possible to obtain consistent meaningful data for the composition and oxidation states of the cations by using a combination of the relevant Mössbauer and phase analyses. To illustrate some of these uncertainties some calculations were carried out for the bulk phase of sample DB125. These calculations are shown in Appendix H.

Also shown in Figure 47 are lamellae observed in the bulk phase. The composition of these lamellae as given by point b in Figure 47 was calculated as follows (oxygen content normalised to 2):

$$Fe_{0.01}Al_{0.01}V_{0.01}Mg_{0.01}Ti_{1.04}O_2$$

There are a total of 1.08 cations for every 2 oxygen atoms. It should be noted that besides the oxygen analysis problem discussed earlier, these lamellae are thin (approximately 10 µm) and therefore difficult to analyse without some interference from the matrix which can influence the analysis.

3.5.2 RESULTS OBTAINED FROM THE TESTWORK WITH MINIATURE SLAG BLOCKS

3.5.2.1 Isothermal testwork on the miniature slag blocks

Sample DB123 was used as starting material for this testwork. The chemical composition of this sample is shown in Table 23. X-ray diffraction patterns of these samples are given in Appendix I.

A) Results of the testwork at 800 °C

The block sample treated at 800 °C for 24 hours (DB124) contained three distinct zones. These zones were as follows:

- The first zone is the outer rim zone. This zone can be seen in Figure 48. Iron migration occurred towards the outer margins of the slag block. This zone is characterised by alternate dense and porous sub-zones.

Figure 48: Photograph of the outer rim of a miniature block sample treated at 800 °C for 24 hours (sample DB124)

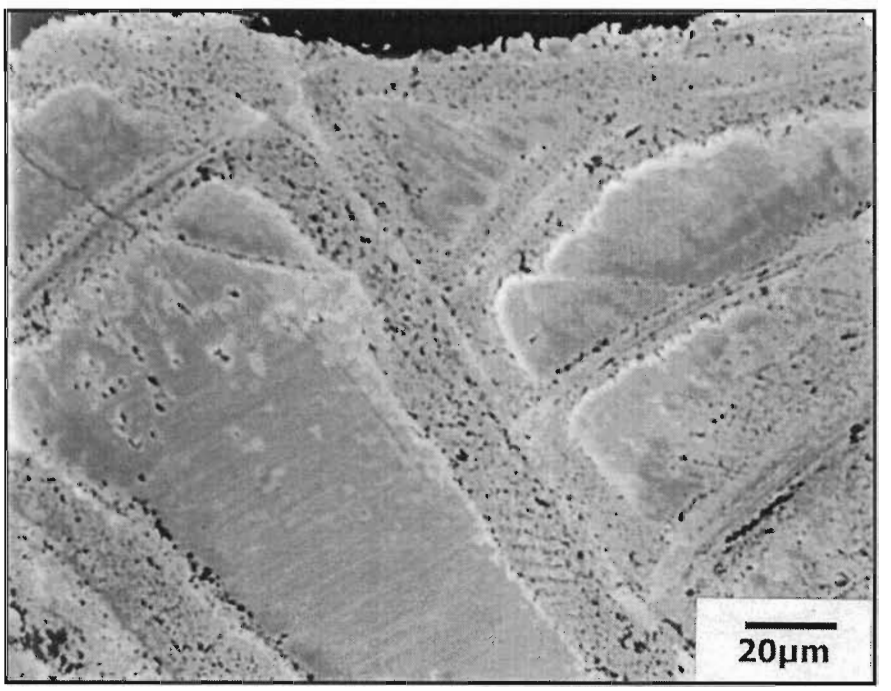

- The second zone is the mantle zone. This zone can be seen in Figure 49. The zone consists predominantly of a mixture of TiO_2 (darker colour) and the M_3O_5-solid solution phase, with abundant fine-grained iron enriched M_3O_5-precipitates (whitish coloured) concentrating along cracks. This zone is not that clearly distinguishable from the outer rim zone.
- The third zone is the core of the block, with the zone being approximately 1 mm in length. This is shown in Figure 50. The core is finely porous and contains an abundance of fine metallic iron precipitates. The core is in general dual phased, consisting of a mixture of

TiO_2 and the M_3O_5-solid solution phase. The metallic iron (bright white) is in general associated with TiO_2.

Figure 49: Photograph of the mantle zone of a miniature block sample treated at 800 °C for 24 hours (sample DB124)

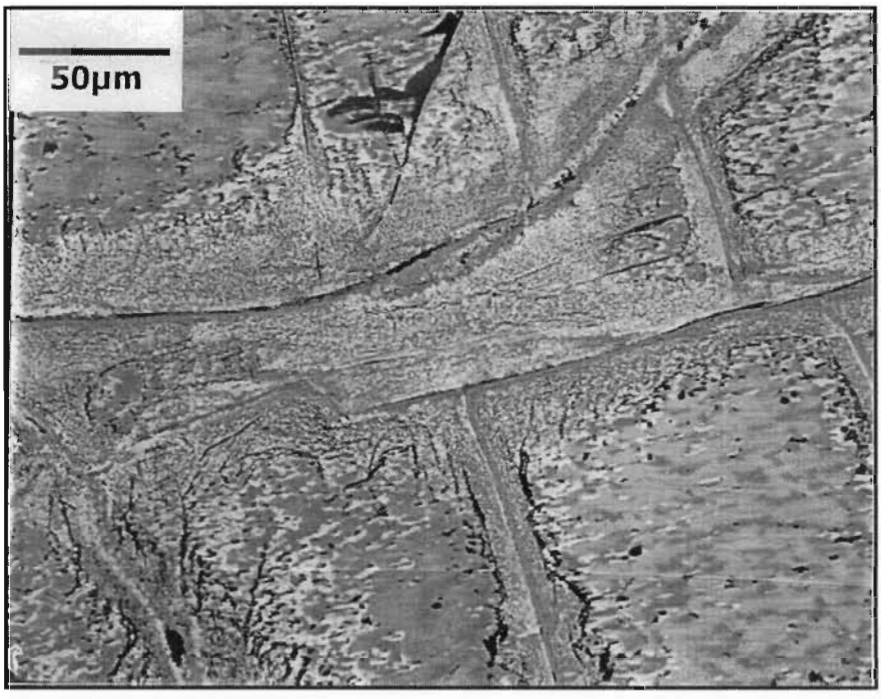

Figure 50: Photograph of the core of a miniature block sample treated at 800 °C for 24 hours (sample DB124)

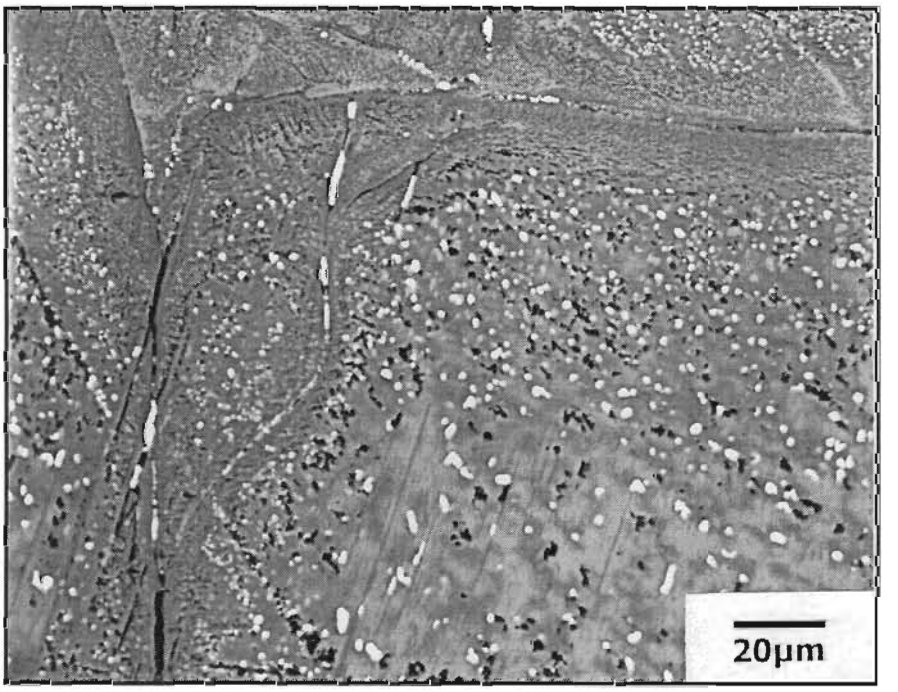

Mössbauer spectroscopy (see Table 29) of the sample shows the presence of pseudobrookite and ilmenite. Ilmenite was also confirmed by X-ray diffraction as indicated by the peaks with

Table 29: Summary of results obtained from Mössbauer spectroscopy for a miniature block sample heated at 800 °C

Sample no.	Temperature (°C)	Time (hours)	Hyperfine interaction parameters			Abundance (atom %)	Attribution
			Isomeric shift - δ ($mm.s^{-1}$)	Quadropole splitting - Δ ($mm.s^{-1}$)	B_{hf} (T)		
DB124	800	24	0.35	0.62	-	41 (3)	Fe^{3+} compound (pseudobrookite)
			1.08	3.05	-	20 (2)	Fe^{2+} compound (ferropseudobrookite)
			1.11	0.70	-	39 (2)	Ilmenite-like compound (Fe^{3+})

Errors are quoted as percentage (in parenthesis)
B_{hf} – internal magnetic field

2θ-values of 23.8, 35.5 and 53.2 degrees (see Appendix I). Rutile was identified as the main phase present, with M_3O_5 as a secondary phase. No decrepitation of this sample was observed.

When comparing sample DB124 with the equivalent pellet sample (24 hours at 800 °C, DB109) several differences are noted:

- The visual appearances of the samples are different (compare Figure 40 with Figure 48, Figure 49 and Figure 50), with sample DB124 showing an elaborate zoned structure.
- From the Mössbauer results sample DB124 contains ilmenite (also confirmed by X-ray diffraction analysis), while sample DB109 contains a hematite-like phase.

B) Results of the testwork at 400 °C

X-ray diffraction patterns for the miniature block samples treated at 400 °C are shown in Appendix I. These results show that the main phases present in these samples are M_3O_5 (or a structural modification there-of) and rutile. Some anatase might also be present. No broad peak at a 2θ-value of approximately 21.1 degrees was observed for these samples (see Appendix G for comparison with the pellet samples). The diffraction patterns of the miniature slag blocks do seem to indicate that the samples after treatment are more amorphous than the starting material. This can be seen by the broadening of the peaks, as well as the increase in the noise levels of the background. It is also noticeable that the miniature block samples contain a significant amount of rutile, while the pellet samples contained a negligible amount of rutile. Another difference between these two types of samples is the disappearance of the M_3O_5 peak at a 2θ-value of 32.5 degrees for the pellet samples, while this peak is still found in the diffraction patterns for the miniature slag blocks. A summary of the peak intensities of the miniature slag blocks is shown in Table 30.

Table 30: A summary of the relative peak intensities for various miniature block samples treated at 400 °C for various times

Sample no.	Time (Hours)	2θ-value (degrees)	Intensity of the peak at a 2θ-value of ~ 25.5 degrees	2θ-value (degrees)	Intensity of the peak at a 2θ-value of ~ 32.5 degrees	$I_{2\theta=32.5}/I_{2\theta=25.5}$
DB123	0	25.7	1691.1	32.7	1042.7	0.617
DB130	6	25.8	1393.7	32.8	666.6	0.478
DB131	24	25.8	551.9	32.8	252.0	0.457
DB133	96	25.7	1174.8	32.7	322.5	0.275
DB132	384	25.7	1155.0	32.7	290.8	0.252

A comparison between the relative intensities of the pellet samples and the miniature block samples are given in Figure 51. The following differences in Figure 51 can be noted:

- It seems that the rate of change of the peak intensity ratio of the blocks is smaller than that of the pellets. This can be seen by comparing the results of the two types of samples obtained after 24 hours. For the pellet samples it is evident that the relative peak intensity is already at a minimum value of 0.076 (14.7 per cent of the value obtained for the starting

material), while for the miniature block sample a value of only 0.457 (74.1 per cent of the value obtained for the starting material) was obtained.

- It also seems that the miniature blocks reach equilibrium at a higher peak ratio level than the pellet samples. For the pellet sample reacted at 384 hours a value of 0.070 (13.5 per cent of the value obtained for the starting material) was obtained, while for the miniature block sample reacted at 384 hours a value of 0.252 (40.8 per cent of the value obtained for the starting material) was obtained.

Figure 51: A comparison of the peak intensity ratios ($I_{2\theta=32.5}/I_{2\theta=25.5}$) for the pellet and miniature block samples treated at 400 °C.

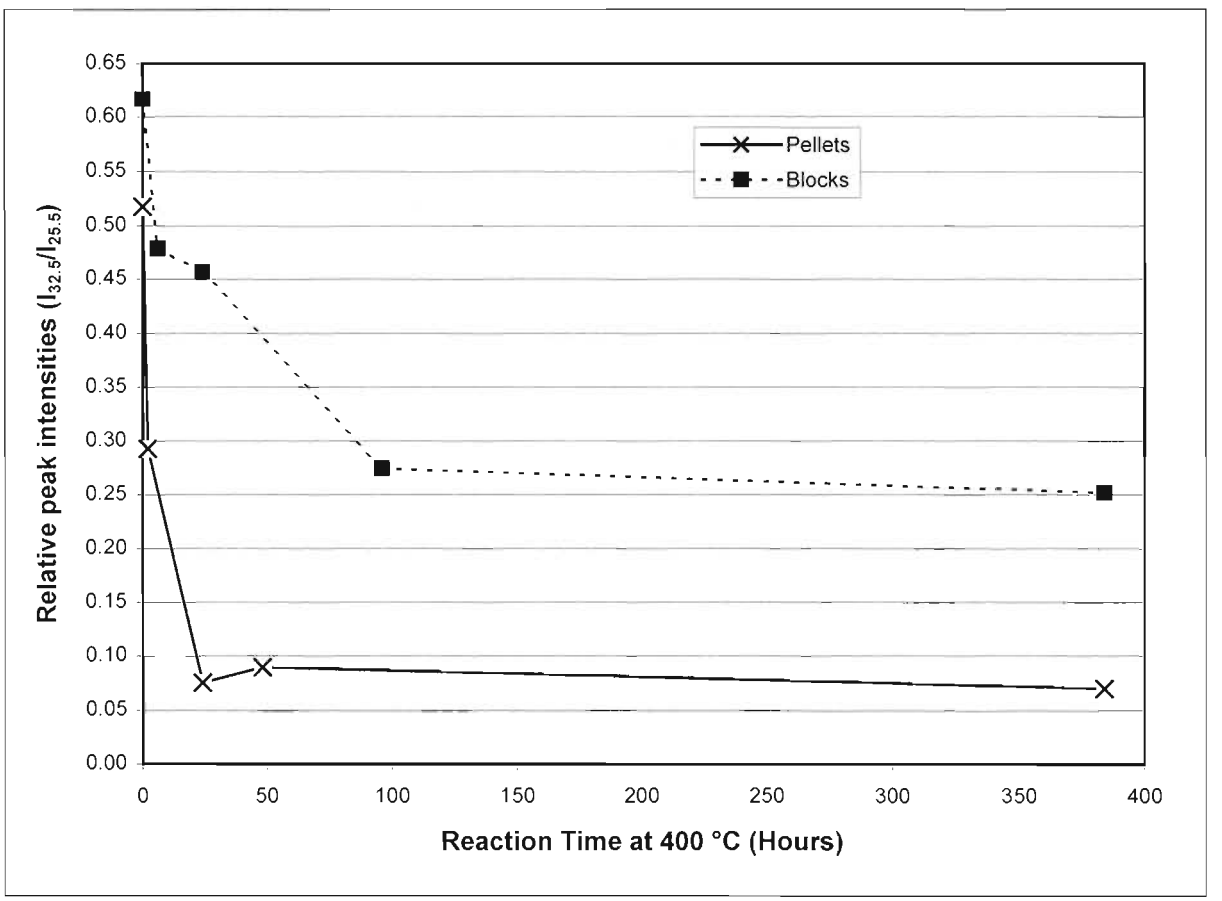

In explaining the different results obtained between the two types of samples, the following differences between the two types of samples should be noted:

- The pellet samples has a higher porosity than that of the miniature block samples. This can result in higher reaction rates if oxygen transfer plays a limiting role in the respective reactions. This is unlikely, given the long reaction times used.
- The chemistry of the respective starting materials is also different. This is shown in Table 23. For the pellet samples the starting material (DB100) contained 9.8 per cent FeO, while the starting material for the miniature block samples (DB123) contained 14.4 per cent FeO. This is considered to be the more likely cause.

The chemistry of the respective starting materials probably also explains the differences between the pellet and miniature block samples obtained at 800 °C, as discussed earlier.

The photograph of the miniature slag block sample heated for 6 hours at 400 °C (DB130) is shown in Figure 52. The photograph displays a section of the block consisting predominantly of the M_3O_5 solid solution phase containing abundant fine-grained, needle-like rutile exsolution lamellae displaying preferred orientation. Cracking of the block can be observed. It should be noted that the cracks do not in any way seem to be associated or aligned with the rutile needles, with some rutile needles even divided into smaller fragments due to cracking perpendicular to the needles. Figure 53 shows a photograph of a sample treated for 96 hours at 400 °C (DB133). Once again extensive cracking of the sample can be observed. The composition of the bulk phase of the block sample treated for 384 hours was as follows (oxygen content normalised to 5):

$$Fe_{0.55}\ Al_{0.03}\ V_{0.01}\ Mg_{0.04}\ Zr_{0.01}\ Ti_{2.29}\ O_{5}$$

It was not possible to determine the oxidation states of the various cations, as no data on the Fe^{2+} and Fe^{3+} content of the sample was available (Mössbauer spectroscopy was not carried out on the sample). There is a total of 2.96 cations for every 5 oxygen atoms in this phase (i.e. close to stoichiometric M_3O_5).

The composition of the rutile phase for the sample DB132 was determined to be as follows (oxygen content normalised to 2):

$$Ti_{1.03}O_2$$

Figure 52: Photograph of a miniature block sample treated at 400 °C for 6 hours (sample DB130)

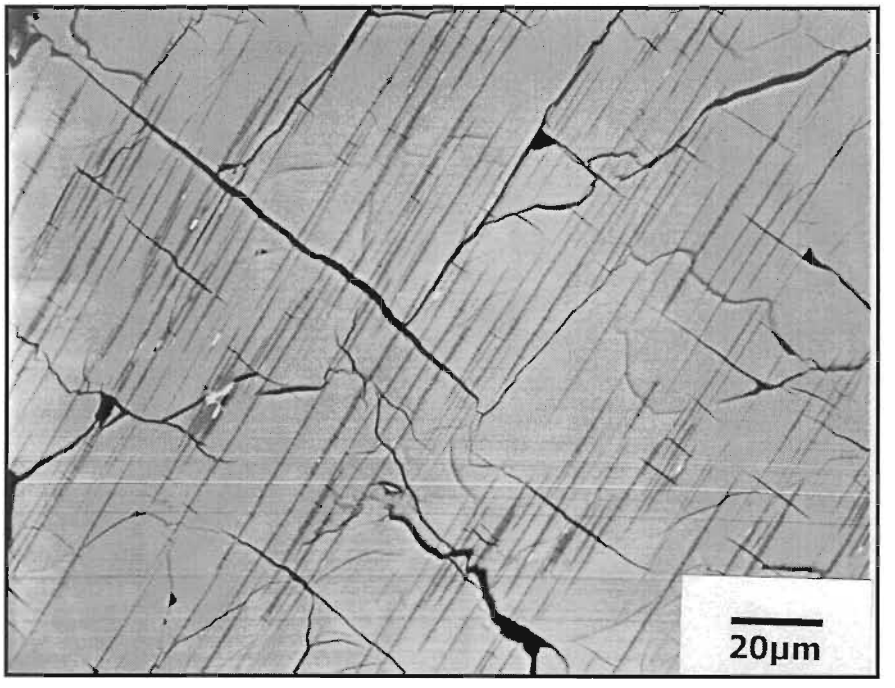

Figure 53: Photograph of a miniature block sample treated at 400 °C for 96 hours (sample DB133)

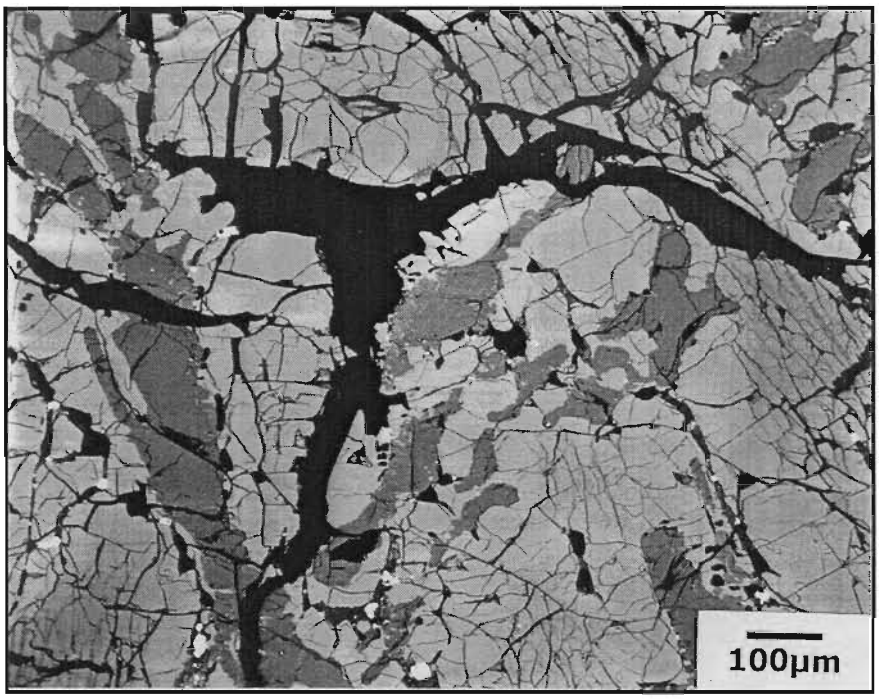

Only limited decrepitation of these miniature slag blocks treated at 400 °C was observed. For the sample treated for 6 hours (DB130) no decrepitation was observed, while for the samples treated for 24 and 96 hours (DB131 and DB133 respectively) only decrepitation on the surface of the blocks were observed. For the sample treated for 384 hours the block broke in two pieces on quenching, indicating a decrease in the strength of the block. However, compared to the pellet samples the observed decrepitation was mild.

3.5.2.2 Results of the unidirectional crushing tests

In an attempt to quantify the effect of decrepitation on the physical strength of the slag it was decided to carry out unidirectional crushing tests on some miniature slag blocks. The starting composition of these blocks is given in Table 23 (sample DB136). The data from the crushing tests were converted to obtain information on the following aspects:

- The total crushing energy for each experimental condition.
- The maximum force required for crushing the blocks for each experimental condition.
- The size distribution of the miniature slag blocks after crushing.

Details of the raw data, and the conversion of the data, is given in Appendix J. Also shown in Appendix J is a statistical analysis of the data.

Figure 54 shows a typical result for the displacement of the miniature slag block as a function of time, while Figure 55 shows the force applied as a function of time for the same sample. This block was treated for 24 hours at 600 °C. Approximately 8 seconds after the recording of data was started, the moving plate was set in motion (see point A; Figure 54). After approximately 10 seconds the miniature slag block made contact with the fixed plate (at point

B in Figure 54). Between points B (10.0 s; 7.1 mm) and C (10.5 s; 6.2 mm) the rate of displacement decreases markedly, with a displacement of only 0.9 mm measured between the two points. This small displacement is related to the increase in the applied force, which causes elastic deformation of the test frame. At point C it seems that the block fractures due to the stress placed on it, with the majority of the material falling away. Point C also coincides with the maximum applied force (see Figure 55). The displacement between points C and D (10.6 s; 2.1 mm) is 4.1 mm. Between points D and E no displacement of the moving plate takes place. This can be explained by a certain amount of play present in the equipment. Between points C and D the moving plate shoots forward due to the release of the pressure when the block fractures. After a time delay (approximately 0.5 seconds in this instance) the slack is taken up again and the moving plate starts moving forward again at point E.

For comparison purposes the graphs obtained for a sample treated at 800 °C for 24 hours are shown in Figure 56 and Figure 57. The major difference between the samples seems to be the maximum force required for the samples (6.13 kN compared to 4.70 kN), indicating that the sample treated at 800 °C is much harder to crush.

Figure 58 shows a summary of the results obtained for the various experimental conditions. The statistical analyses done in Appendix J show that only the following significant differences between the various experimental conditions with regard to the total energy required for crushing were calculated:

- The samples treated at 800 °C for 24 hours required significantly more energy to crush than the other samples.

The following results between the various experimental conditions were found with regard to the maximum force applied to the miniature slag blocks:

- The untreated slag samples required significantly less force to crush than the samples treated at 600 °C for 24 hours and the samples treated at 800 °C for 24 hours.
- The samples treated at 600 °C for 24 hours required significantly more force to crush than the samples treated at 600 °C for 96 hours.
- The samples treated at 600 °C for 24 hours required significantly less force to crush than the samples treated at 800 °C for 24 hours.
- The samples treated at 600 °C for 96 hours required significantly less force to crush than the samples treated at 800 °C for 24 hours.
- No significant difference in the force required for crushing the blocks were found between the untreated slag samples and the samples treated at 600 °C for 96 hours.

The size distributions of the slag blocks after crushing were also evaluated. The percentage slag less than 500 μm was used as indicator. These results are shown in Figure 59. The following significant results were obtained:

- The untreated slag samples contained significantly more –500 μm material after crushing than the samples treated at 600 °C for 24 and 96 hours, as well as the samples treated at 800 °C for 24 hours.
- The samples treated at 600 °C for 24 hours also contained significantly more –500 μm material than the samples treated at 600 °C for 96 hours and the samples treated at 800 °C for 24 hours.

No significant difference in size between the samples treated at 600 °C for 96 hours and the samples treated at 800 °C for 24 hours were found.

Figure 54: Displacement of the miniature slag block treated at 600 °C for 24 hours as a function of time (test no. 6241)

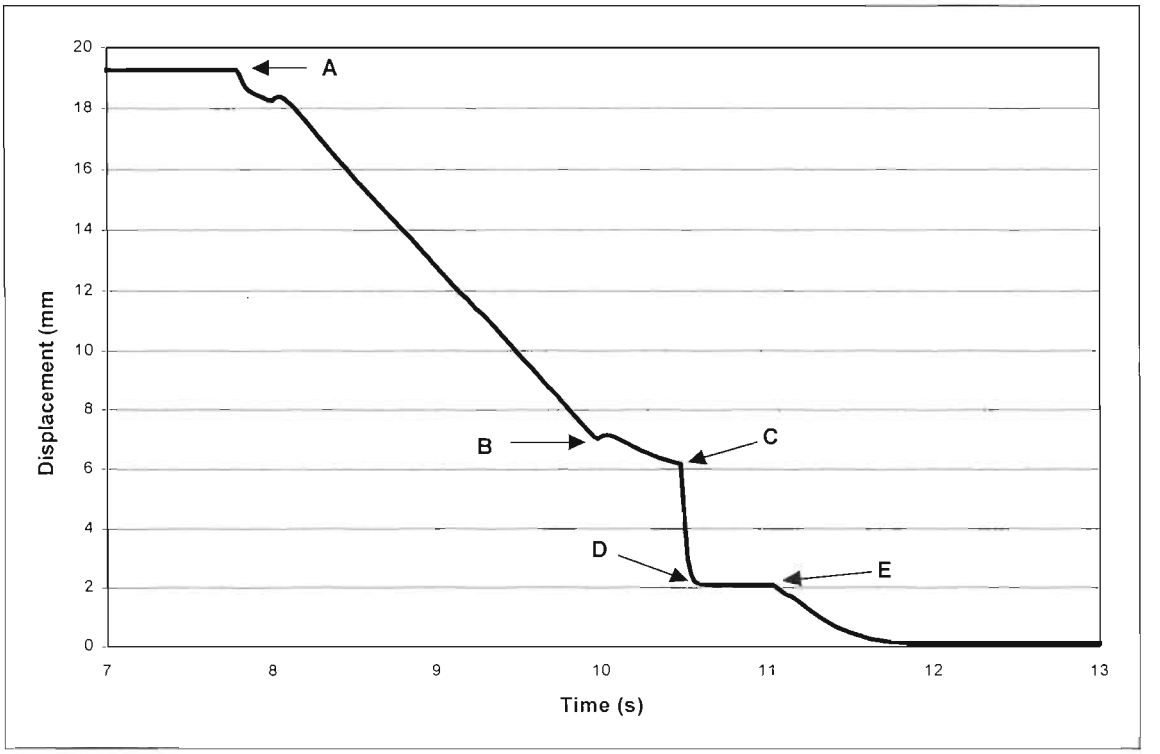

Figure 55: Measurement of the force applied as a function of time for a miniature slag block treated at 600 °C for 24 hours (test no. 6241)

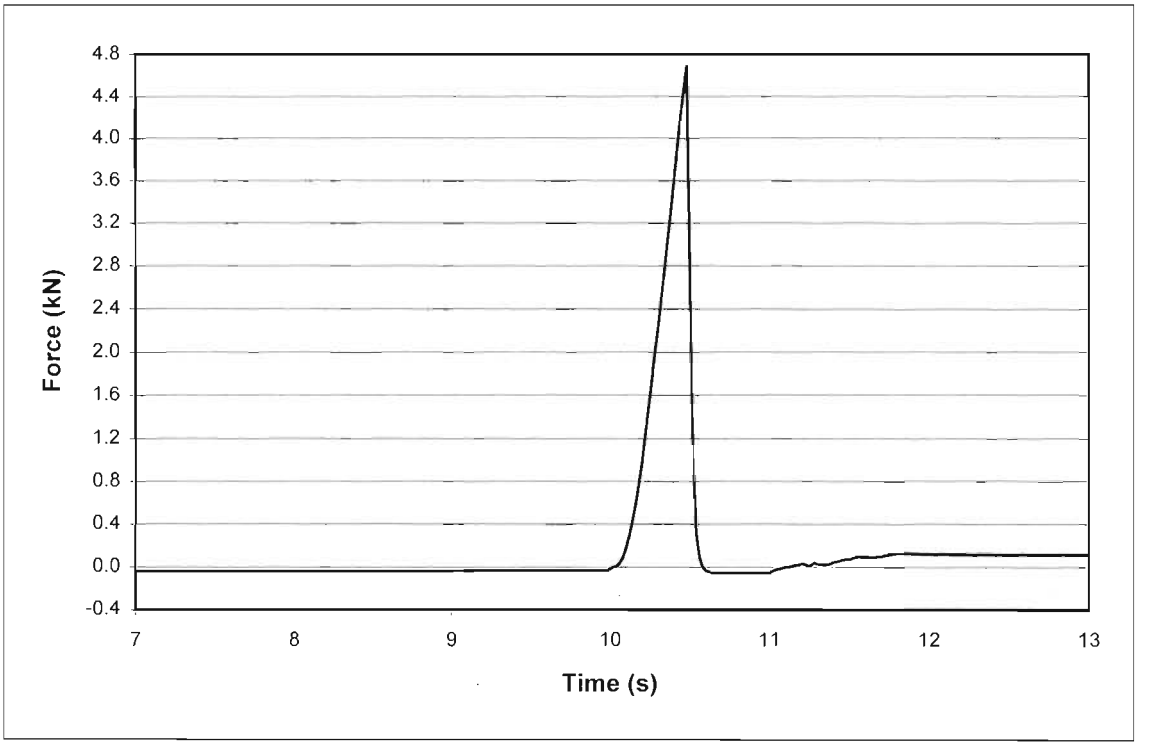

Figure 56: Displacement of the miniature slag block treated at 800 °C for 24 hours as a function of time (test no. 8243)

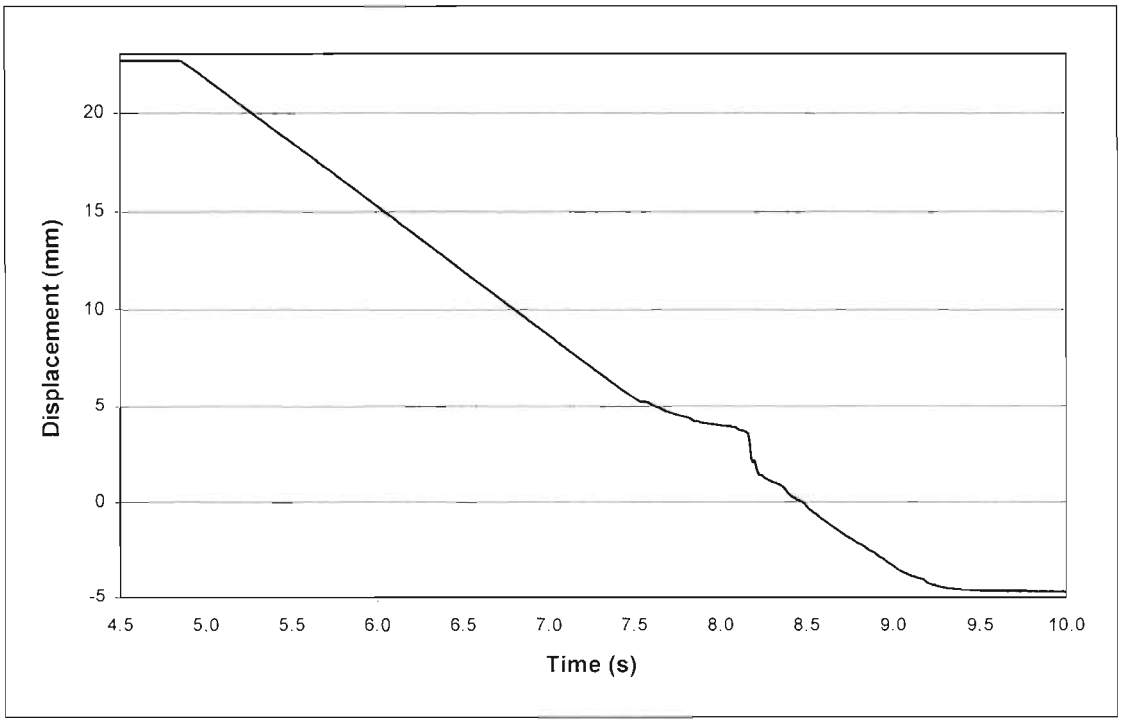

Figure 57: Measurement of the force applied as a function of time for a miniature slag block treated at 800 °C for 24 hours (test no. 8243)

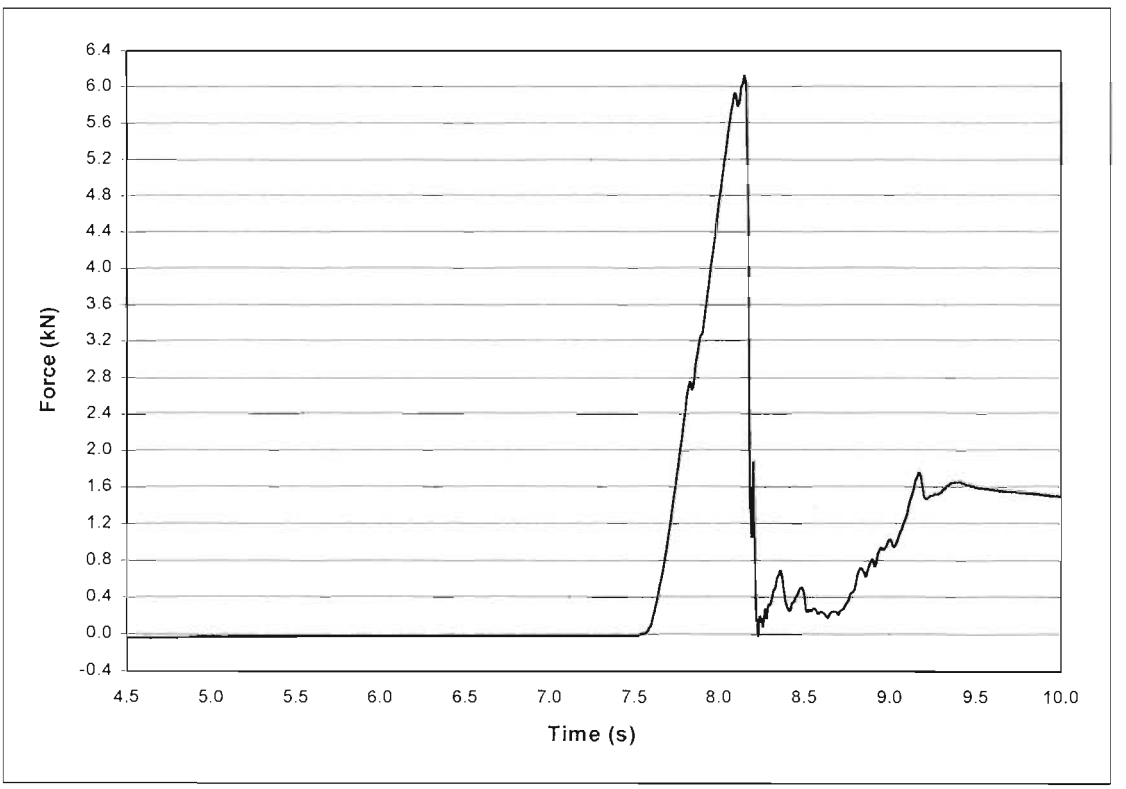

Figure 58: The total energy required and the maximum force applied for the crushing of the miniature slag blocks

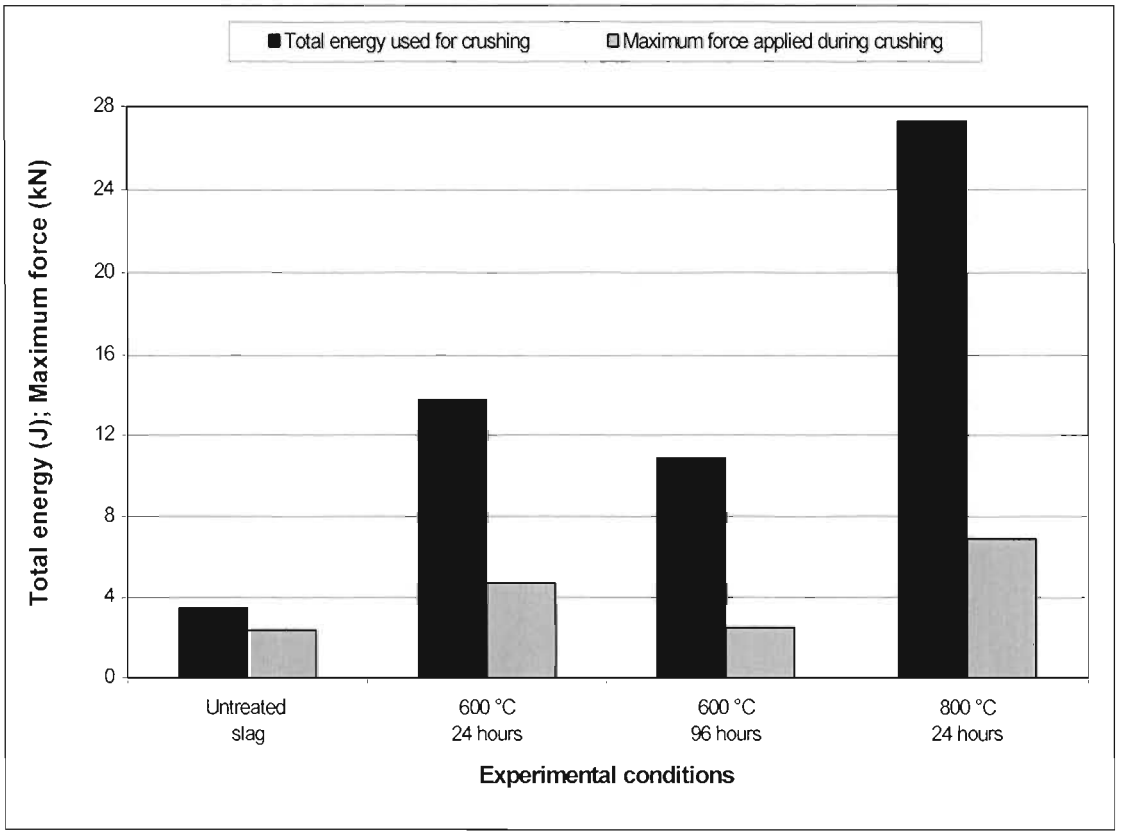

Figure 59: Size distribution of the miniature slag blocks after the crushing tests

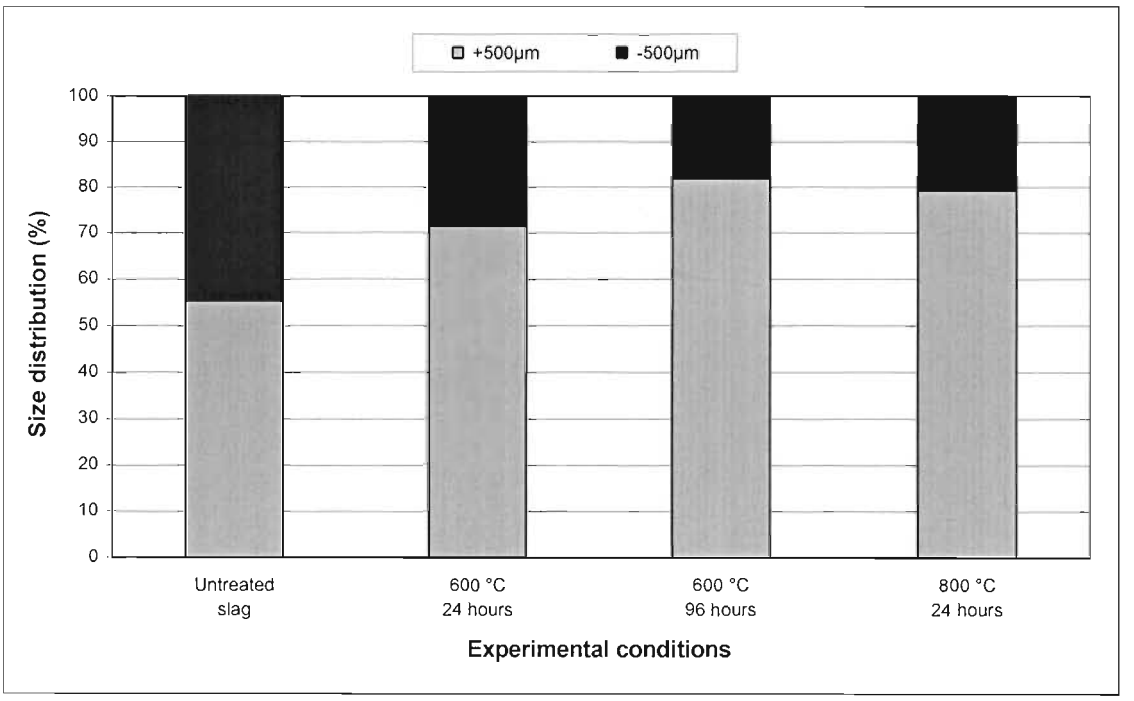

It was only possible to carry out crushing tests on the miniature slag blocks treated at 600 and 800 °C as the blocks treated at 400 °C decrepitated completely on quenching. This was somewhat surprising, as the miniature slag blocks discussed in the previous section (starting material DB123, see Table 23 for composition) did not decrepitate on quenching. X-ray diffraction data from one of the samples prepared for 24 hours at 400 °C for the crushing testwork are given in Appendix K. The sample was separated into two size fractions after decrepitating on quenching. Sample DB145 represents the –1 mm size fraction, while sample DB146 represents the +1 mm size fraction. Also shown in Appendix K is the X-ray diffraction pattern for the –212 μm size fraction one of the untreated slag samples (DB139, slag 2 as shown in Table 46, Appendix J).

The size fraction was obtained subsequent to the crushing test. Sample DB139 is essentially the starting material for samples DB145 and DB146. Once again the broad peak at a 2θ-value of approximately 21.1 degrees is observed for samples DB145 and DB146, indicating the presence of the M_6O_{11} phase. This peak was also found in the pellet samples treated at 400 °C, but not for the miniature block samples treated at 400 °C discussed in the previous section.

The likely explanation of the different results is therefore the difference in chemical composition of the respective starting materials. The samples that showed the appearance of the M_6O_{11} phase contained 9.8 and 8.4 per cent FeO in their respective starting materials (see samples DB100 and DB136, Table 23), while the samples that did not show this phase contained 14.4 per cent FeO in their starting material. This sample obviously also contains the least amount of Ti^{3+}. It appears that the formation of the M_6O_{11} phase is driven by the oxidation of Ti^{3+} to Ti^{4+} at low temperatures in the M_3O_5 structure. It seems that the formation of the M_6O_{11} phase is sensitive to the composition of the slag, with the slag containing 14.4 % FeO being too iron-rich for the M_6O_{11} phase to form in significant amounts.

3.5.3 RESULTS FROM TESTWORK IN DIFFERENT ATMOSPHERES

For the tests carried out in different atmospheres sample DB100 in the form of a powder was used as starting material. The experimental conditions of the tests are shown in Table 31, with the chemical analyses of the various samples given in Table 32. Where Ar+Air is indicated as the atmosphere, it indicates experiments that were carried out in the reactor where it was subsequently discovered that a leak was present in the system. Also shown in Table 31 is a summary of the results extracted from the X-ray diffraction patterns (patterns given in Appendix L). As described previously the $I_{2\theta=32.5}/I_{2\theta=25.5}$ ratio is again taken as an indication of the presence of the M_3O_5 phase. The Ti_2O_3 content of the samples in Table 32 is taken as the extent of oxidation of the samples. Thus for the starting material (DB100) the Ti_2O_3 content was determined to be 30.4 per cent, while for the sample heated in air for 72 hours the Ti_2O_3 content was analysed as being less than 1 per cent. At these low levels of Ti_2O_3 it could also be expected that all or most of the iron would be oxidised to Fe^{3+}, with similar results that could be expected for the pellet and miniature slag block samples treated under similar conditions. No Mössbauer spectroscopy analysis was however carried out on these samples. The samples heated in Ar+Air showed an intermediate level of oxidation, with Ti_2O_3 levels of approximately 20 per cent. The sample treated only in Ar also showed some oxidation, with a Ti_2O_3 level of 26.4 per cent compared to 30.4 per cent for the starting material. The possibility

Table 31: A summary of the relative peak intensities for samples treated in various atmospheres

Sample no.	Temperature (°C)	Time (Hours)	Atmosphere	2θ-value (degrees)	Intensity of the peak at a 2θ-value of ~ 32.5 degrees	2θ-value (degrees)	Intensity of the peak at a 2θ-value of ~ 25.5 degrees	$I_{2\theta=32.5}/I_{2\theta=25.5}$
DB100	Starting material			25.6	3021.6	32.8	1564.7	0.518
DB196	400	24	Ar	25.2	472.6	32.4	214.5	0.454
DB186	400	24	Ar+Air	25.5	504.5	32.7	203.3	0.403
DB185	370	24	Ar+Air	25.2	414.0	32.4	152.5	0.368
DB184	400	24	Air	25.2	426.3	32.3	115.0	0.270
DB193	400	48	Air	25.4	378.4	32.4	24.5	0.065
DB194	400	72	Air	25.3	376.5	32.3	24.1	0.064

Table 32: Analyses of the samples treated in various atmospheres

Sample no.	Analyses (mass %)												
	SiO_2	Al_2O_3	CaO	MgO	MnO	Cr_2O_3	V_2O_5	ZrO_2	Fe^0	FeO	TiO_2	Ti_2O_3	Total Ti as TiO_2
DB100	1.41	1.19	0.27	1.03	1.17	0.05	0.45	0.16	< 0.1	9.80	53.9	30.4	87.70
DB196	1.81	1.18	0.25	1.27	1.14	0.10	0.45	-	< 0.1	9.79	57.6	26.4	
DB186	1.46	1.14	0.27	1.24	1.09	0.10	0.45	-	< 0.1	9.61	65.0	21.5	
DB185	1.32	1.12	0.25	1.24	1.08	0.09	0.46	-	< 0.1	9.54	67.1	18.6	
DB184	1.50	1.16	0.27	1.25	1.11	0.10	0.46	-	< 0.1	9.58	70.4	14.9	
DB193	1.78	1.16	0.28	1.21	1.09	0.09	0.43	-	< 0.1	9.45	85.3	< 1	
DB194	1.72	1.11	0.23	1.17	1.06	0.09	0.42	-	< 0.1	9.19	85.3	< 1	

that some air leakage into the experimental set-up occurred to cause this oxidation can not be excluded. Ti_2O_3 can of course also be oxidised by Fe^{2+} in the disproportionation reaction that has been mentioned several times.

Evaluating the results obtained in Table 31 and Table 32, a direct correlation between the extent of oxidation and the decrease in the M_3O_5 content (as exemplified by the decrease in the $I_{2\theta=32.5}/I_{2\theta=25.5}$ ratio) becomes apparent. This is illustrated in Figure 60. Also shown is a linear regression fit with a R^2 value of 0.99, indicating the excellent correlation obtained. Comparing samples DB196 (treated for 24 hours in Ar) and DB184 (treated for 24 hours in air), the latter appears to have a substantial number of cracks compared to sample DB196.

These results also provide a possible solution for preventing the decrepitation of titania slags. From the results it can be inferred that decrepitation can be avoided if the slag is cooled down under an inert atmosphere. This will probably only be necessary at relatively low temperatures of less than 600 to 700 °C.

Figure 60: Correlation between the Ti_2O_3 content and the ratio of X-ray diffraction intensities at 2θ-values of 32.5 and 25.5 degrees

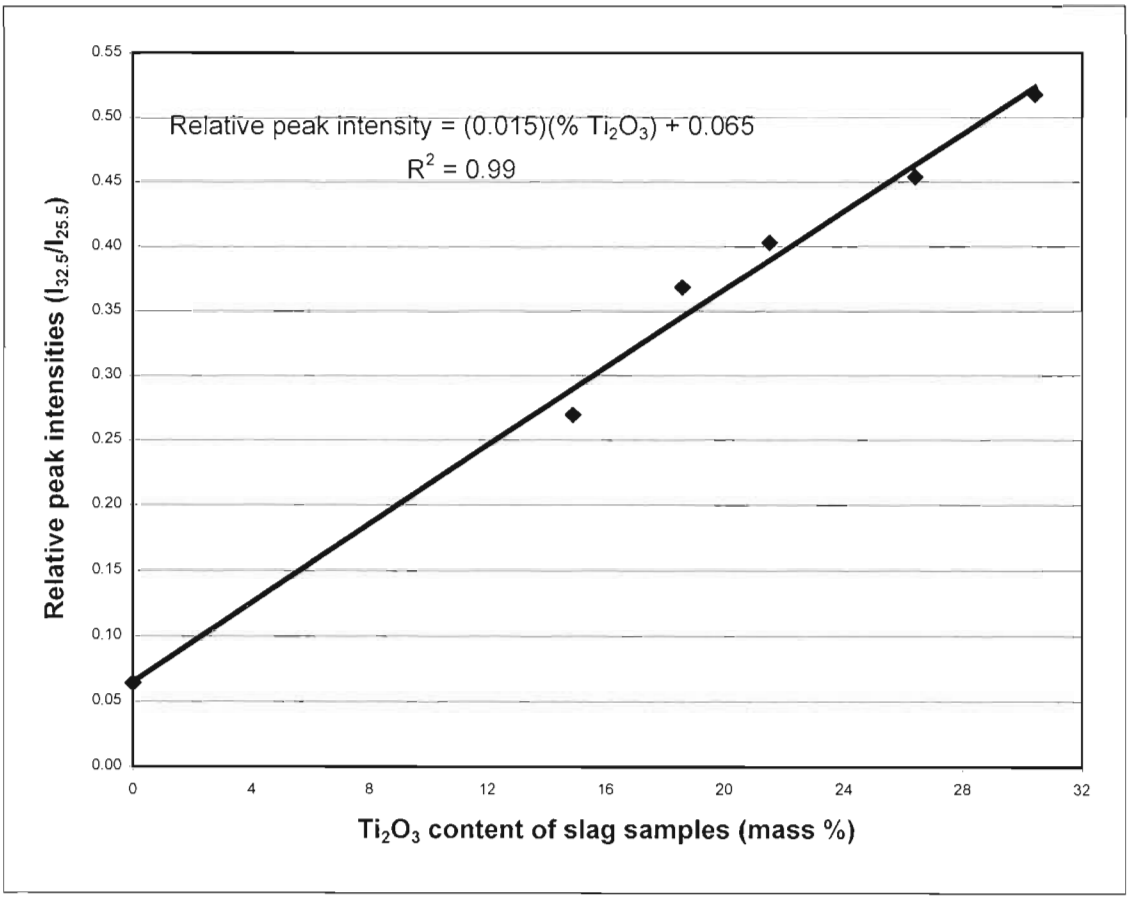

3.5.4 RESULTS FROM THE DATA OBTAINED DURING THE MAY 2000 SMELTING CAMPAIGN

The decrepitation phenomenon on large, slow-cooled slag blocks during the smelting campaign was studied, as this closely approximates the situation that could be expected on an industrial scale plant. In this campaign decrepitated slag was obtained directly from cooled liquid slag. This is different to the small-scale tests described previously, where quenched liquid slag was re-heated at various temperatures in order to study decrepitation. This part of the study is therefore also important in assessing the relevance of the small-scale testwork.

It also appears from observations that the decrepitation of the slag blocks is a relatively low temperature phenomenon. Decrepitation of the blocks only seemed to occur after the blocks had stopped glowing red, possibly indicating that the decrepitation reactions only occur at temperatures below 700-800 °C. This corroborates the results obtained from the small-scale tests, where significant decrepitation of the titania slag was only obtained below 600 °C.

3.5.4.1 Cooling rate of slag blocks

The temperature measurements obtained for the cooling of the two slag blocks are shown in Figure 61. The calculated cooling rates for the two slag blocks are also shown in Figure 62. Due to the protective sheath configurations (described previously) enclosing the thermocouples, the response time of the thermocouples were relatively slow. For tap 73, 63 minutes elapsed (after the closing of the taphole) before the maximum temperature of 1654 °C was registered. This is a difference of 18 °C when compared to the measured tap temperature of 1672 °C. For tap 79, 76 minutes elapsed (also relative to the closing of the taphole) prior to registering a maximum temperature of 1662 °C. This is a difference of 14 °C when compared to the tap temperature of 1676 °C.

The cooling rate of tap 79 was higher than that of tap 73, despite tap 79 (1029 kg) being approximately sixteen per cent larger than tap 73 (889 kg). The chemical compositions of the two taps are fairly similar, and it is not expected that this would make a significant difference in the respective cooling rates. The analyses of the two slags are shown in Table 33. The difference in the cooling rates can rather be explained by the relative position of the thermocouple assemblages in the slag blocks. The positions of the thermocouple assemblages for the two taps are shown in Figure 63. From the diagrams it is evident that the thermocouple assemblage for tap 79 is much closer to the bottom of the ladle, a distance of 157 mm compared to 245 mm for tap 73. It was also calculated that the closest distance to the side of the ladle for tap 79 was approximately 244 mm, while for tap 73 this distance was approximately 301 mm. It therefore seems reasonable to expect the measured cooling rate of tap 79 to be faster than those of tap 73. The maximum cooling rates of between 2 and 2.2 °C per minute for the blocks were attained after 8 to 10 hours. After this the cooling rates of the blocks decreased rapidly, with values of less than 0.2 °C per minute obtained at the completion of the measurements.

Very little interaction between the SiC thermocouple sheath material and titania slag was found (For details see Appendix M). It can therefore be recommended that these types of sheaths again be used in future for similar applications.

Figure 61: Temperature measurements obtained for the cooling of two slag blocks

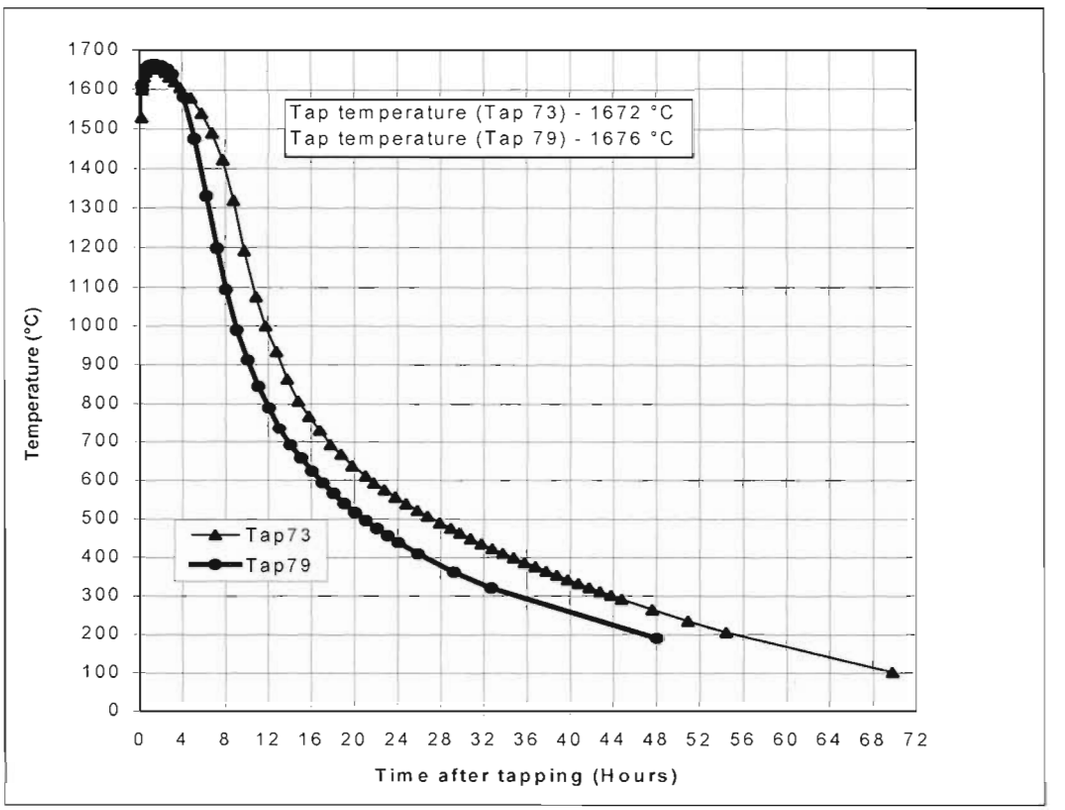

Figure 62: Cooling rates calculated for the two slag blocks

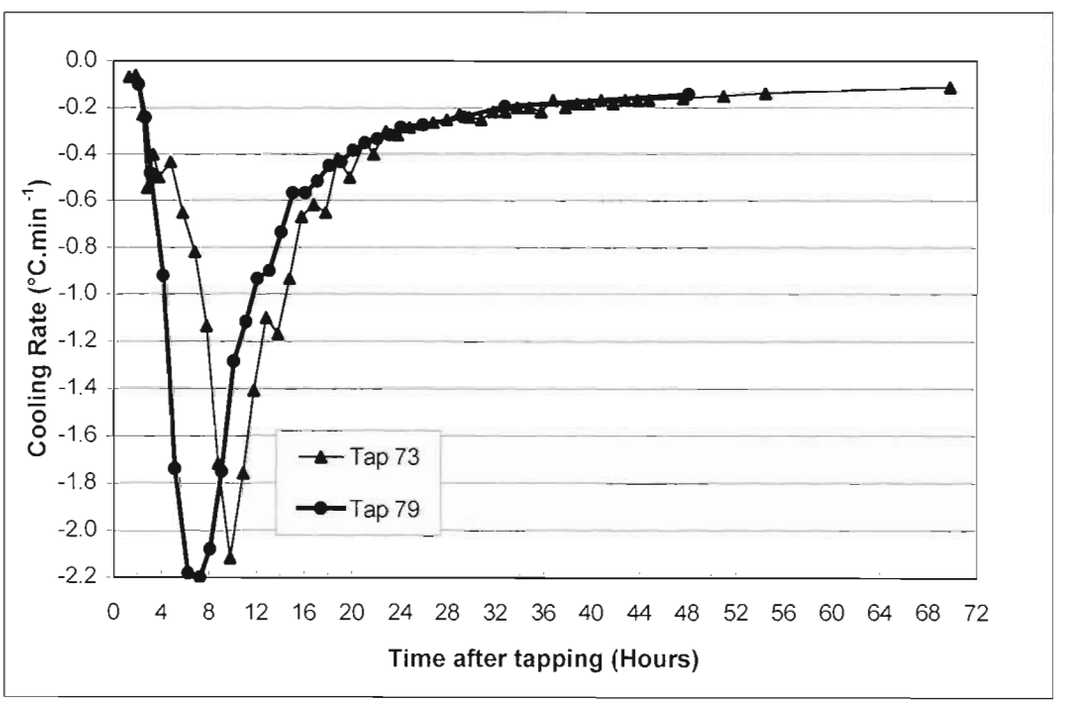

Table 33: Chemical analyses of taps 73 and 79

Tap no.	Chemical analyses (mass %)								
	SiO_2	Al_2O_3	CaO	MgO	MnO	Cr_2O_3	V_2O_5	Total Fe as FeO	Total Ti as TiO_2
73	1.62	1.33	0.26	0.94	1.25	0.11	0.46	10.90	85.94
79	1.65	1.40	0.27	1.01	1.29	0.11	0.45	9.26	87.36

Figure 63: Positioning of the thermocouple assemblages in the slag ladles for determining the cooling rate of the slag taps (not drawn to scale)

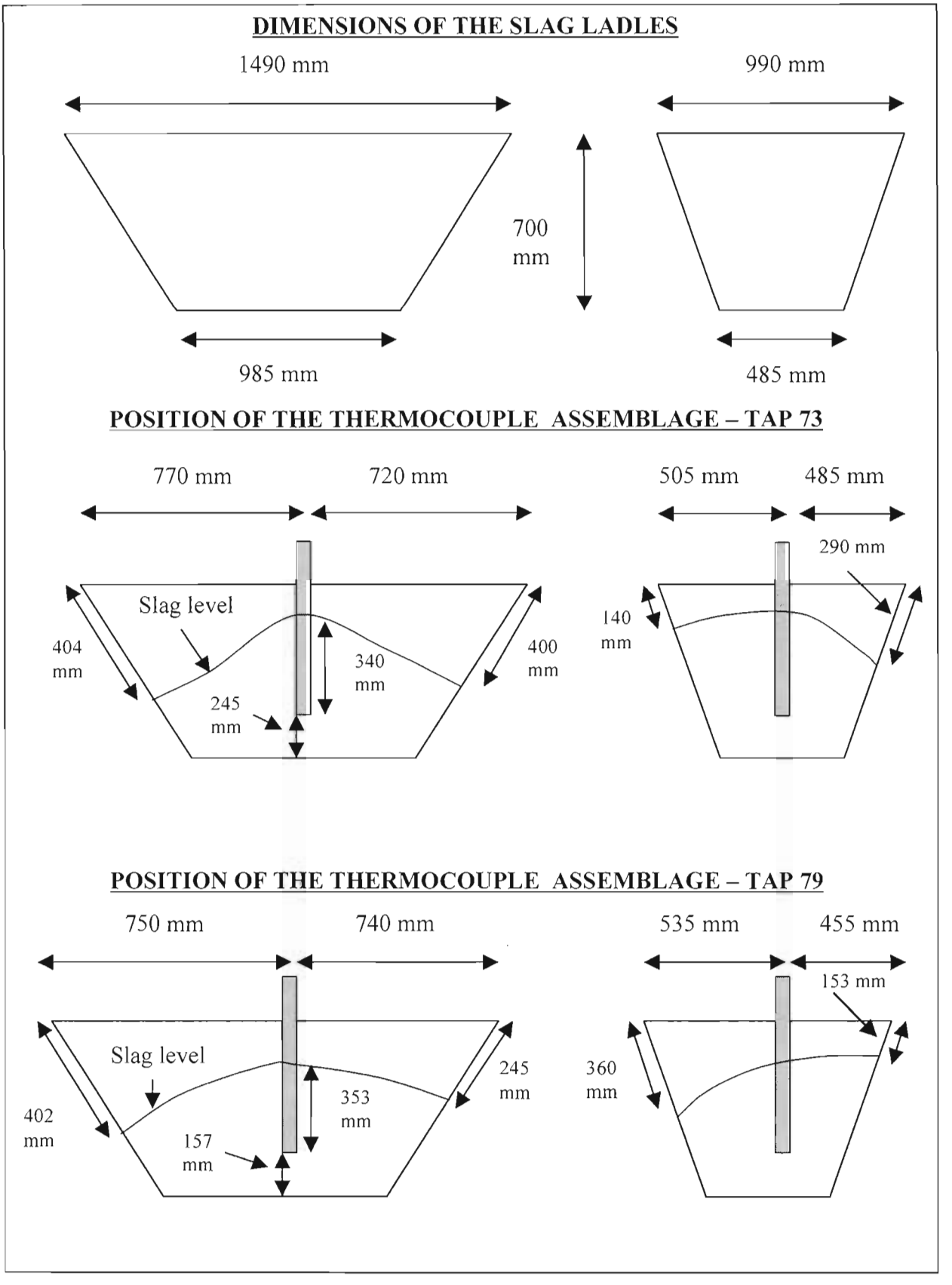

3.5.4.2 Characterisation of decrepitated slag samples from slag blocks

Decrepitated slag samples were obtained from two slag blocks, tap 68 and tap 70. Figure 64 and Figure 28 show different views of tap 68 to illustrate the effect of decrepitation on these large slag blocks. It can be seen that a substantial portion of the block had decrepitated, with the slag material crumbling away. In the background of Figure 28 a ladle can be seen of the type into which slag was tapped.

The chemical analyses of the various samples obtained from taps 68 and 70 are shown in Table 34 and Table 35. In each instance a sample obtained from the tap stream was analysed. Samples of the decrepitated material were taken after different intervals from different locations of the decrepitated slag blocks. Mössbauer analyses were also carried out on the samples (see Table 36 and Table 37). The Mössbauer results were used to calculate the Fe^{3+} content of the slags where applicable. It is apparent from the analyses that the decrepitated material had undergone some oxidation. This can be seen by the decrease of the Ti_2O_3 content of the slags over a period of time. This is illustrated clearly in Figure 65. At the lower Ti_2O_3 content levels it was found that Fe^{2+} had also started to oxidise to Fe^{3+}. This can be seen for example for sample DB155 in Table 34.

A micrograph of decrepitated sample DB157 (description and analysis given in Table 35) is shown in Figure 30. The similarities with the pellet samples treated at 400 °C is striking (see Figure 45 and Figure 46), with all the samples showing extensive cracking.

Figure 64: Front view of a slag block (tap 68) that had decrepitated

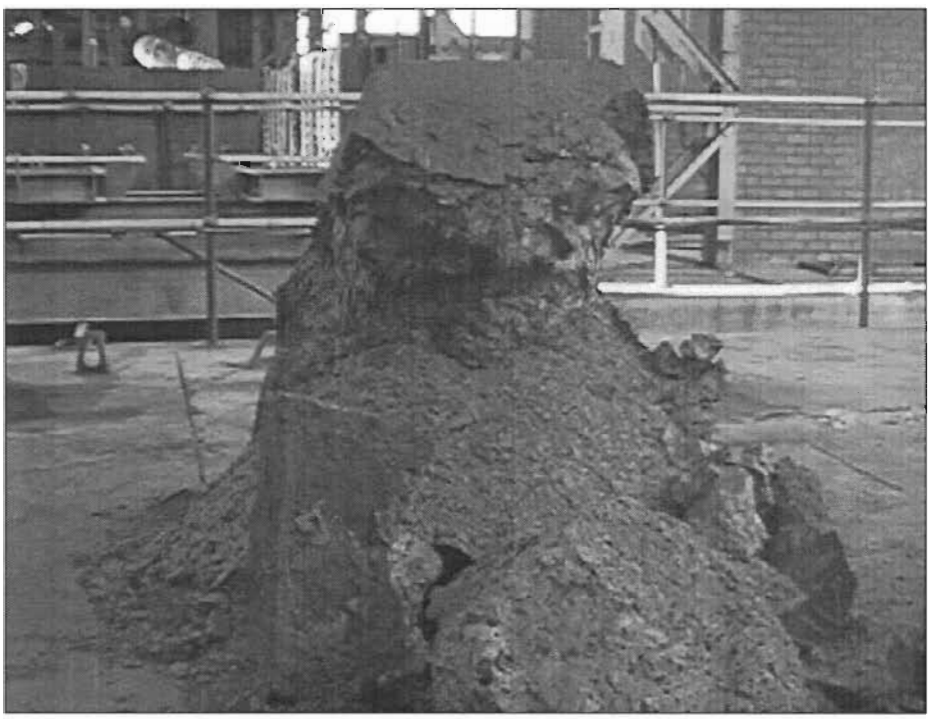

Table 34: Analyses of decrepitated slag samples taken from tap 68

Analyses no.	Origin of Sample	Analyses (mass %)													
		SiO_2	Al_2O_3	CaO	MgO	MnO	Cr_2O_3	V_2O_5	Fe^0	FeO	Fe_2O_3	TiO_2	Ti_2O_3	Total Ti as TiO_2	Insoluble TiO_2 content
DB152	Tap stream	1.76	1.64	0.24	1.02	1.40	0.09	0.42	0.39	6.83	-	48.4	36.78	89.29	0.71
DB153	Wide side of block (16.6 hours after tapping)	1.65	1.62	0.22	1.31	1.30	0.09	0.41	0.13	7.58	-	64.0	17.71	83.70	3.24
DB154	Narrow side of block (16.2 hours after tapping)	2.21	1.60	0.27	1.11	1.42	0.08	0.39	0.18	7.28	-	61.9	22.97	87.40	3.76
DB155	Narrow side of block (36.7 hours after tapping)	2.70	1.57	0.34	1.10	1.70	0.10	0.33	0.16	7.40	1.23	72.4	9.69	83.20	5.39

Table 35: Analyses of decrepitated slag samples taken from tap 70

Analyses no.	Origin of Sample	Analyses (mass %)													
		SiO_2	Al_2O_3	CaO	MgO	MnO	Cr_2O_3	V_2O_5	Fe^0	FeO	Fe_2O_3	TiO_2	Ti_2O_3	Total Ti as TiO_2	Insoluble TiO_2 content
DB156	Tap stream	1.84	1.48	0.27	1.07	1.33	0.09	0.43	0.19	9.42	-	52.0	30.92	86.40	1.04
DB157	Wide side of block (36.7 hours after tapping)	1.73	1.43	0.25	1.06	1.23	0.09	0.43	0.28	8.45	0.81	76.6	8.07	85.60	0.69

Table 36: Mössbauer analyses of the decrepitated samples taken from tap 68

Sample number	Sample origin	Hyperfine interaction parameters			Abundance (atom %)	Attribution
		Isomeric shift - δ ($mm.s^{-1}$)	Quadropole splitting - Δ ($mm.s^{-1}$)	B_{hf} (T)		
DB152	Tap stream	1.07 (3)	3.00 (5)	-	75 (5)	Fe^{2+} compound (ferropseudobrookite; site A)
		1.07 (2)	1.85 (3)	-	25 (4)	Fe^{2+} compound (ferropseudobrookite; site B)
DB153	Wide side of block (16.6 hours after tapping	1.07 (3)	3.06 (4)	-	65 (5)	Fe^{2+} compound (ferropseudobrookite; site A)
		1.03 (4)	1.90 (5)	-	35 (5)	Fe^{2+} compound (ferropseudobrookite; site B)
DB154	Narrow side of block (16.2 hours after tapping)	1.08 (2)	3.0 (2)	-	62 (4)	Fe^{2+} compound (ferropseudobrookite; site A)
		1.04 (3)	1.90 (5)	-	38 (5)	Fe^{2+} compound (ferropseudobrookite; site B)
DB155	Narrow side of block (36.7 hours after tapping)	1.07 (2)	3.08 (2)	-	41 (4)	Fe^{2+} compound (ferropseudobrookite; site A)
		1.00 (3)	2.0 (5)	-	46 (5)	Fe^{2+} compound (ferropseudobrookite; site B)
		0.49 (3)	0.68 (2)	-	13 (3)	Fe^{3+} compound (pseudobrookite)

Errors are quoted as percentage (in parenthesis)

Table 37: Mössbauer analyses of the decrepitated samples taken from tap 70

Sample number	Sample origin	Hyperfine interaction parameters			Abundance (atom %)	Attribution
		Isomeric shift - δ ($mm.s^{-1}$)	Quadropole splitting - Δ ($mm.s^{-1}$)	B_{hf} (T)		
DB156	Tap stream	1.08 (2)	3.03 (3)	-	82 (5)	Fe^{2+} compound (ferropseudobrookite; site A)
		1.04 (3)	2.0 (5)	-	15 (5)	Fe^{2+} compound (ferropseudobrookite; site B)
		0.49 (3)	0.68 (2)	-	3 (3)	Fe^{3+} compound (pseudobrookite)
DB157	Wide side of block (36.7 hours after tapping	1.07 (2)	3.0 (2)	-	65 (5)	Fe^{2+} compound (ferropseudobrookite; site A)
		1.04 (2)	1.69 (3)	-	27 (3)	Fe^{2+} compound (ferropseudobrookite; site B)
		0.49 (3)	0.68 (2)	-	8 (5)	Fe^{3+} compound (pseudobrookite)

Errors are quoted as percentage (in parenthesis)

Figure 65: The Ti_2O_3 content of decrepitated campaign slag samples taken at various times

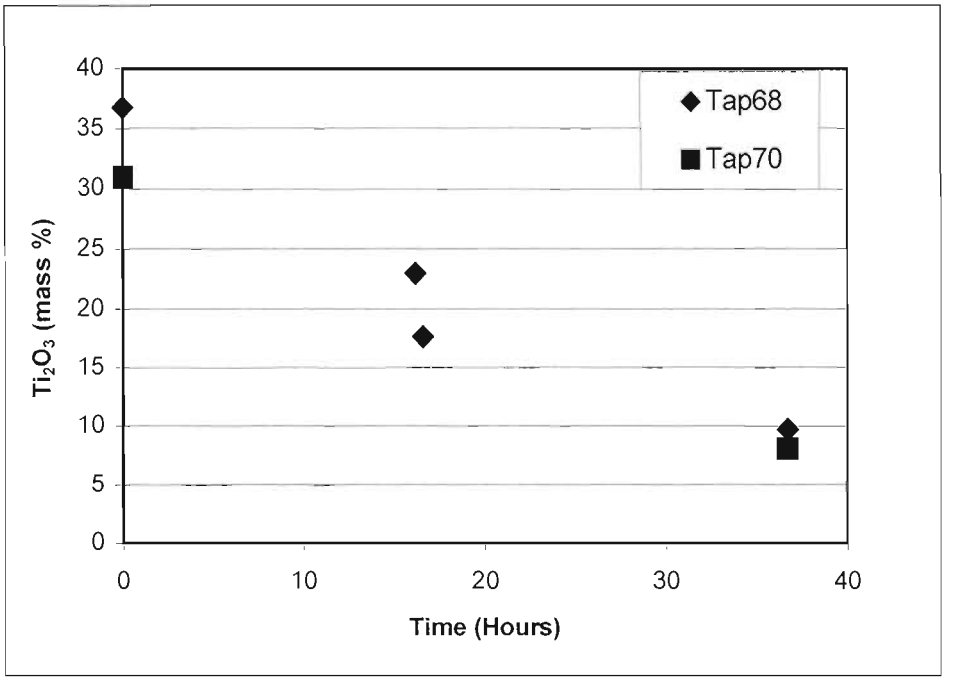

The insoluble TiO_2 content of the decrepitated samples was also analysed. These results give an indication of the insoluble content of the slag for the sulphate processing route. The maximum insoluble content specification for the sulphate processing route is 4 per cent. For tap 68 the insoluble content increases as the slag is oxidised, with a value of 5.4 per cent obtained for the most oxidised sample. For tap 70 this relationship is not apparent, with the oxidised slag having a slightly lower value than the starting slag.

The Mössbauer results also show that the distribution of iron in the A and B sites of the structure changes from the starting material to the decrepitated material. This can be seen in Table 36, where 75 per cent of the iron for the tap stream sample (DB152) is in the A site, with the remainder in the B site. For decrepitated sample DB154 it can be seen that only 62 per cent of the iron now resides in the A site, while 38 per cent of the iron is in the B site.

X-ray diffraction patterns of the various decrepitated samples obtained during the smelting campaign are given in Appendix N. Once again it can be seen from the patterns that the decrepitated slag samples appear more amorphous that the starting materials. As with the small-scale testwork it is again observed that the intensity of the peak at approximately 32.5 degrees decreases relative to the intensity of the peak at a 2θ-value of approximately 25.5 degrees. This is shown in Table 38 and Table 39 for taps 68 and 70 respectively. Also noticeable from the X-ray diffraction patterns is the appearance of the broad peak at a 2θ-value of approximately 21 to 22 degrees for the decrepitated samples. This is especially noticeable for sample DB157.

This is similar to the results obtained for the pellet samples treated at 400 °C, where it was postulated that the disappearance of the M_3O_5 phase is associated with the formation of a

M_6O_{11} phase. Based on these results it therefore appears that the small-scale testwork gives similar results to that obtained in the campaign testwork.

Table 38: A summary of the relative peak intensities for the decrepitated slag samples obtained during the campaign from tap 68

Sample no.	Description	2θ-value (degrees)	Intensity of the peak at a 2θ-value of ~ 25.5 degrees	2θ-value (degrees)	Intensity of the peak at a 2θ-value of ~ 32.5 degrees	$I_{2\theta=32.5}/I_{2\theta=25.5}$
DB152	Tap stream	25.2	543.3	32.4	274.7	0.506
DB153	Wide side of block (16.6 hours after tapping)	25.3	400.3	32.4	130.7	0.327
DB154	Narrow side of block (16.2 hours after tapping)	25.2	425.7	32.3	148.7	0.349
DB155	Narrow side of block (36.7 hours after tapping)	25.4	373.3	32.3	53.4	0.143

Table 39: A summary of the relative peak intensities for the decrepitated slag samples obtained during the campaign from tap 70

Sample no.	Description	2θ-value (degrees)	Intensity of the peak at a 2θ-value of ~ 25.5 degrees	2θ-value (degrees)	Intensity of the peak at a 2θ-value of ~ 32.5 degrees	$I_{2\theta=32.5}/I_{2\theta=25.5}$
DB156	Tap stream	25.2	466.4	32.4	256.0	0.549
DB157	Wide side of block (36.7 hours after tapping)	25.4	447.6	32.3	68.0	0.152

Sieve analyses of grab samples taken from the two decrepitated slag blocks (taps 68 and 70) were carried out to get an indication of the size distribution of the decrepitated material. The size distribution results are shown in Table 40 and Figure 66. Approximately 25 per cent of the samples was smaller than 106 µm in size. This is an unacceptably high value. The reason for that is that a size fraction of less than 106 µm is not acceptable for the chloride process for the production of pigment, but only for the sulphate processing route. After the slag cooling process, the slag also undergoes a crushing and milling process. During this process it can be expected that the decrepitated material will be milled finer still, thereby compounding the problem.

The chemical and Mössbauer analyses of two size fractions from tap 68 (see Table 40) are given in Table 41 and Table 42 respectively. These results seem to indicate that the –106 µm size fraction had undergone more change. This is indicated by the slightly lower Ti^{3+} analysis,

as well as the greater disorder of the iron atoms in the various sites as determined by the Mössbauer analysis.

Table 40: Size distribution of decrepitated slag samples obtained from two slag blocks

Sieve fraction (μm)	Tap 68		Tap 70	
	Mass (g)	Percentage (%)	Mass (g)	Percentage (%)
+2000	37.3	4.2	15.1	2.1
-2000+1180	12.2	1.4	4.9	0.7
-1180+850	68.0	7.7	11.2	1.6
-850+600	111.5	12.7	51.6	7.3
-600+425	114.6	13.0	73.9	10.5
-425+300	94.1	10.7	82.2	11.7
-300+212	107.4	12.2	102.6	14.6
-212+150	77.7	8.8	77.5	11.0
-150+106	73.3	8.3	75.0	10.7
-106	185.2	21.0	209.9	29.8
Total	**881.3**	**100.0**	**703.9**	**100.0**

Figure 66: Size distribution of decrepitated slag

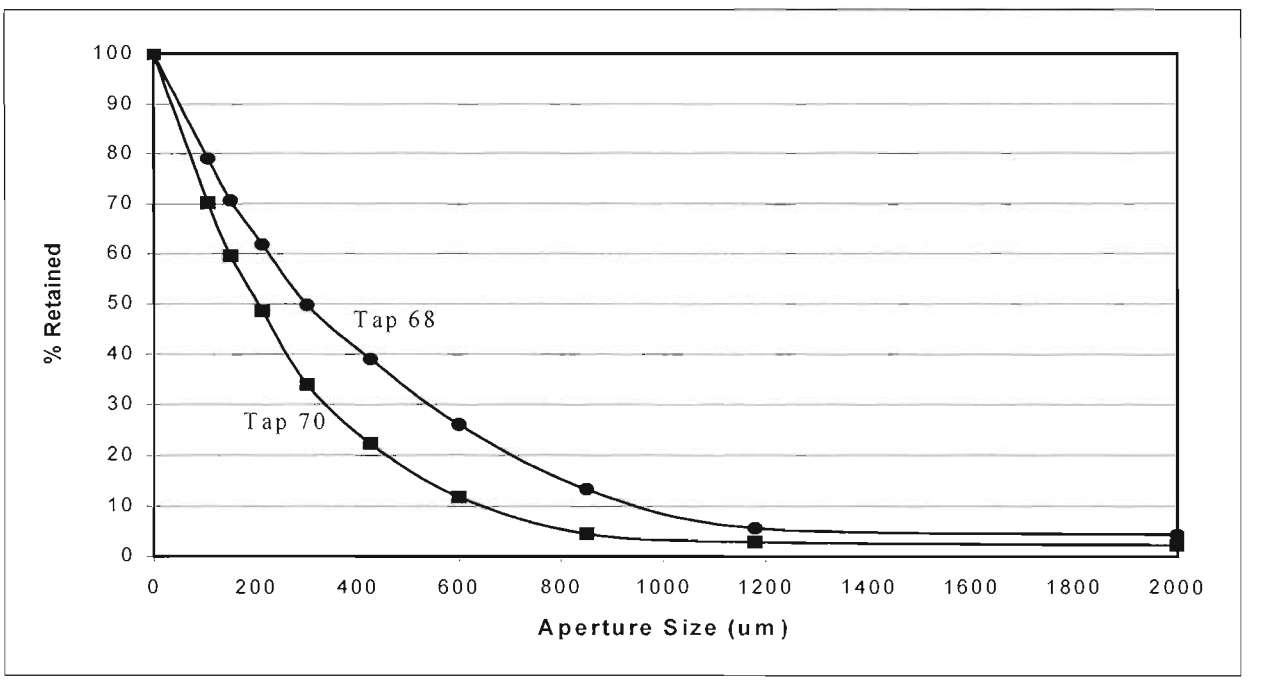

The specific density of some of the decrepitated samples was also determined. Details of these results are shown in Appendix O, with a summary of the results given in Table 43. The estimated uncertainty was based on the following errors:

- The reproducibility of the instrument.
- The sample mass, with a lower sample mass having a larger error.
- The temperature at which the density determinations were carried out.
- The particle size of the samples.

Table 41: Analyses of selected samples obtained from the size distribution analyses shown in Table 40

Analyses no.	Origin of Sample	Analyses (mass %)												
		SiO_2	Al_2O_3	CaO	MgO	MnO	Cr_2O_3	V_2O_5	Fe^0	FeO	Fe_2O_3	TiO_2	Ti_2O_3	Total Ti as TiO_2
DB152	Tap stream	1.76	1.64	0.24	1.02	1.40	0.09	0.42	0.39	6.83	-	48.4	36.78	89.29
DB175	Tap 68, -850+600 µm size fraction	3.24	1.51	0.44	0.87	1.77	0.10	0.30	<0.1	7.63	1.05	76.67	5.76	83.07
DB178	Tap 68, -106 µm size fraction	2.00	1.57	0.28	1.07	1.75	0.10	0.38	<0.1	7.49	2.35	81.92	4.18	86.57

Table 42: Mössbauer analyses of two size fractions obtained from the size distribution analyses shown in Table 40

Sample number	Sample origin	Hyperfine interaction parameters			Abundance (atom %)	Attribution
		Isomeric shift - δ ($mm.s^{-1}$)	Quadropole splitting - Δ ($mm.s^{-1}$)	B_{hf} (T)		
DB152	Tap stream	1.07 (3)	3.00 (5)	-	75 (5)	Fe^{2+} compound (ferropseudobrookite; site A)
		1.07 (2)	1.85 (3)	-	25 (4)	Fe^{2+} compound (ferropseudobrookite; site B)
DB175	Tap 68, -850+600 µm size fraction	1.07 (3)	3.07 (4)	-	62 (5)	Fe^{2+} compound (ferropseudobrookite; site A)
		1.01 (4)	1.85 (5)	-	27 (5)	Fe^{2+} compound (ferropseudobrookite; site B)
		0.30 (2)	0.87 (3)	-	11 (5)	Fe^{3+} compound (pseudobrookite)
DB178	Tap 68, -106 µm size fraction	1.07 (2)	3.04 (3)	-	39 (5)	Fe^{2+} compound (ferropseudobrookite; site A)
		1.07 (3)	2.03 (5)	-	39 (5)	Fe^{2+} compound (ferropseudobrookite; site B)
		0.27 (3)	0.80 (2)	-	22 (3)	Fe^{3+} compound (pseudobrookite)

Errors are quoted as percentage (in parenthesis)

Although the results are not statistically significant based on the estimated uncertainty, there does however seem to be a general trend. Both decrepitated samples DB155 and DB157 seem to have lower densities than their respective starting materials (DB152 and DB156). It is also noticeable that the finer size fraction (DB178) has a lower density than the coarser size fraction. These results do seem to indicate that the decrepitation of titania slag is associated with a change in the density of the slag (and therefore also the volume).

Table 43: Comparison of the densities of decrepitated samples with their respective starting materials

Sample no.	Sample description	Average Density ($g.cm^{-3}$)	Estimated uncertainty ($g.cm^{-3}$)
DB152	Tap stream - tap 68	3.9546	0.028
DB155	Narrow side of block – tap 68 (36.7 hours after tapping)	3.9432	0.092
DB156	Tap stream - tap 70	3.9670	0.028
DB157	Wide side of block – tap 70 (36.7 hours after tapping	3.9397	0.047
DB175#	Tap 68, -850+600 µm size fraction	3.9403	0.028
DB178#	Tap 68, -106 µm size fraction	3.9266	0.028

- Samples obtained from size distribution analyses as shown in Table 40.

3.6 GENERAL COMMENTS, CONCLUSIONS AND RECOMMENDATIONS

From the results obtained in this study it appears that the samples treated at 400 °C had the largest propensity to decrepitate. This propensity to decrepitate decreased markedly with an increase in temperature, with samples treated at 600 °C and higher temperatures showing minimal to no signs of decrepitation. It was found that the microstructure of decrepitated slag samples produced on a laboratory scale were similar to that of the samples obtained from the large-scale slag blocks.

A potential mechanism for the decrepitation of the high titania slags mentioned initially is the possibility of a polymorphic phase change of one of the phases present in the slag. It is for example known that Ti_3O_5 undergoes a reversible phase transformation at 190 °C (Grey and Ward, 1973). In various samples produced by Haggerty and Lindsley (1970) crystals in the pseudobrookite field frequently showed a tendency to form a rim with a lower reflectivity compared to the core. No variation in the iron and titanium concentration was found across the core and the rim in their study. The investigators therefore inferred that the rim represented a quenched polymorphic inversion product of pseudobrookite.

From the results obtained in this study, it seems that a more likely explanation for the decrepitation behaviour is the observed changes in the phase assemblages at temperatures below 600 °C.

As discussed previously, Vasyutinskiy (1968) found that a distortion of the M_3O_5 crystal lattice occurred on oxidation of the slag samples at temperatures of approximately 400 °C. The X-ray diffraction data of Teller et. al. (1990, pp. 351-367) for their samples after heating

also shows distortion of the M_3O_5 crystal structure. The Mössbauer results obtained in this study tend to confirm the idea that the crystal structure of the M_3O_5 phase found in the starting material changes when heated at 400 °C (see Table 27 for results). The Mössbauer spectra shown in Appendix C for example illustrates the differences in the Mössbauer spectra for the starting slag (DB100) and for the pellet sample treated for 384 hours at 400 °C (DB125). The X-ray diffraction results of the severely decrepitated samples indicate the presence of a M_6O_{11} phase. Anatase was also found to be present in these samples. These phases were also previously found by Grey, Cranswick, et. al. (2000) for $Mg_{0.3}Ti_{2.7}O_5$ samples oxidised at these low temperatures. They stated that oxidation of their samples produced new phases of general composition based on unit cell intergrowth of M_3O_5 and anatase structural elements. The structural homogeneity was restricted to regions of approximately 100 to 200 Å, due to the low driving force for ordering at these temperatures. It can be assumed that the decrepitation of the samples at the temperatures below 600 °C is caused by the formation of the large number of cracks observed in these samples. It is postulated that these cracks are formed due to volume changes on formation of these new M_nO_{2n-1} phases. Unfortunately no information was found on the volume changes associated with the oxidation of M_3O_5 to M_6O_{11}. From the density data in Table 43 it seems that the decrepitated material has a lower density, and therefore a higher volume, than that of the starting materials which only contain the M_3O_5 phase.

Based on the above conclusions from this study the question can be asked as to why these M_nO_{2n-1} phases only seem to form at temperatures below 600 °C. This is an aspect for further investigation. The following thoughts suggest that this might be due to kinetic limitations at these low temperatures:

- From the isothermal Fe-Fe_2O_3-TiO_2 phase diagrams presented by Borowiec and Rosenqvist (1981) it was concluded for temperatures as low as 650 °C, Fe_2TiO_5 and TiO_2 should be the phases attained at equilibrium for the oxidation of titania slag (see for example Figure 35 for the diagram at 650 °C). No data was however available at lower temperatures.
- As discussed earlier (see reaction (M)) it is also well known that Fe_2TiO_5 decomposes at 585 °C to form Fe_2O_3 and TiO_2 (Haggerty and Lindsley, 1970). This is also illustrated in Figure 37 for the Ti_3O_5-Fe_2TiO_5 system. It can therefore be suggested that at low temperatures the equilibrium phases after complete oxidation of titania slag should be M_2O_3 and TiO_2 phases. From the data of Haggerty and Lindsley (1970) this should be at a temperature of below 585 °C. As seen earlier the effect of impurities on the stability of the M_3O_5 phase probably plays a significant role in the determination of this decomposition temperature.
- For sample DB125 it was however found that this "equilibrium" is not attained after heating the particular pellet sample for 16 days at 400 °C in air. This is indicated by the presence of Ti^{3+} and Fe^{2+} in the bulk phase as found from data from the elemental analyses and Mössbauer data for this sample. From the X-ray diffraction results M_6O_{11} and anatase are the major phases present.
- At temperatures above 600 °C the expected equilibrium phases are different, with ferric pseudobrookite and TiO_2 to be expected. After heating samples for 16 days at temperatures of 800 and 1000 °C these were indeed found to be the main phases present. At 600 °C rutile and anatase was identified as the main phases present, with the M_3O_5 phase almost completely disappearing.

From the temperature measurements of the slag blocks during cooling it was established that from tapping, the slag blocks took approximately 18 to 24 hours to cool down to 550 °C (see

Figure 61). To cool down from 550 to 200 °C approximately another 30 hours was required, providing ample time for partial oxidation of the slag. It also seems that when decrepitation of the slag at these temperatures is initiated, the decrepitated material breaks off from the block, thereby exposing fresh slag to the atmosphere for further oxidation.

An aspect that warrants further investigation is the effect of the chemistry of the starting slag on the decrepitation of the slag. It seems from the results of this study that the propensity to decrepitate decreases with an increase in the FeO content of the slag and a decrease of the Ti_2O_3 content of the slag. The reason for this is not understood at this stage.

Another aspect that warrants further work is the application of Mössbauer spectroscopy in understanding the transformations that occur. In this study the data obtained on the decrepitated slags was modeled as having a pseudobrookite structure. In some instances the X-ray diffraction results showed that the M_3O_5 phase had disappeared, with a M_6O_{11} phase forming. The interpretation of the Mössbauer data in the light of the X-ray diffraction data therefore needs to be confirmed. It is still possible that the Mössbauer data is applicable, as the local environment of the iron atoms in the two phases could be similar. Another interesting aspect that was noted with the Mössbauer investigations was the increase in the line width from the starting materials to that of the decrepitated material. According to Hearne (2000) this can probably be ascribed to increasing disorder in the structure of the M_3O_5 phase. This was however not followed up in this study.

4 ACKNOWLEDGEMENTS

The author would like to make the following acknowledgements:

- Professors Kobus Geldenhuis and Chris Pistorius for their inputs and encouragement during the study.
- Corelie Visser and Leonie Reyneke with their assistance with X-ray diffraction and mineralogical investigations.
- Dr. Giovanni Hearne and Dr. Antoine Mulaba for carrying out the Mössbauer spectroscopy.
- Dr. Villie Viljoen and co-workers for carrying out the electron microprobe analyses.
- Professor Johan de Villiers and Dr. Johan Nell for interesting and useful discussions.
- Iscor for providing me with the opportunity to do this study.
- The Innovation fund (Project no. 32215) of the South African Department of Arts, Culture, Science and Technology for partial funding of the project.
- My family (Robyn, Mark and Gail) for their patience and support over the last couple of months while I was completing the study.

5 REFERENCES

Akimoto S., Nagata T. and Katsura T. "The $TiFe_2O_5$-Ti_2FeO_5 solid solution series", *Nature, Vol. 179, No. 4549, 5 January 1957, pp. 37-38.*

Anderson A.T., Bunch T.E., Cameron E.N., Haggerty S.E., Boyd F.R. Finger L.W., James O.B., Keil K., Prinz M., Ramdohr P. and El Goresy A. "Armalcolite: A new mineral from the Apollo 11 samples", *Proceedings of the Apollo 11 Lunar Science Conference, Vol. 1, 1970, pp.55-63.*